Applied Thermal Engineering 236 (2024) 121473

Contents lists available at ScienceDirect

Applied Thermal Engineering

journal homepage: www.elsevier.com/locate/apthermeng

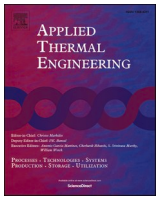

Research Paper

Experimental evaluation of the CO_2-based mixtures CO_2/R32, CO_2/R1234yf and CO_2/R1270 in a transcritical refrigerating plant considering the effect of the internal heat exchanger (IHX)

D. Sánchez *, R. Larrondo, F. Vidan-Falomir, R. Cabello

Jaume I University, Dep. of Mechanical Engineering and Construction, Campus de Riu Sec s/n, E-12071 Castellón, Spain

ARTICLE INFO

Keywords:
CO_2
COP
Zeotropic mixtures
R32
R1270
R1234yf

ABSTRACT

Using CO_2 mixtures results in a simple but effective solution to increase the critical temperature of CO_2 and reduce its working pressures. However, the overall effect of these mixtures on the global performance of the cycle has yet to be explored experimentally in detail. Accordingly, this work tests three CO_2-binary blends with R32, R1270 and R1234yf in a small-capacity vapour compression test rig considering the same working conditions of heat rejection temperature and cooling demand. These mixtures were compared with pure CO_2 in two-cycle arrangements without and with the internal heat exchanger (IHX). The results without IHX provided COP enhancements of *6.4%*, *9.7%* and *15.3%* with CO_2/R1270, CO_2/R1234yf and CO_2/R32, respectively, compared to CO_2 without IHX. Using the IHX and taking CO_2 without IHX as a reference, the COP increments ranged from *6.7%* with R744, *12.1%* with CO_2/R1270, 16.1% with CO_2/R1234yf and *22.2%* with CO_2/R32.

1. Introduction

Due to the high environmental impact caused by the hydrofluorocarbons (HFCs), the European Commission approved 2014 regulation No 517/2014, known as F-Gas, to phase out refrigerants with high values of global warming potential (GWP) [1]. The main consequence of this regulation promoted the development of the 4th refrigerant generation based on unsaturated organic compounds known as hydrofluoroolefins (HFOs) and the recovery of the 1st refrigerant generation composed of natural substances such as hydrocarbons, ammonia or carbon dioxide. Thanks to its non-flammability, safety, and good heat transfer properties, carbon dioxide (CO_2 or R744) has been widely extended, providing services to *18.4%* of the total European stores in 2022, where *90.1%* of them were equipped with centralised refrigeration systems, and only *9.9%* were supplied with condensing units [2]. However, this growth is limited by the high investment cost of CO_2 transcritical units due to the implementation of advanced control systems and complex architectures [3–5] to overcome the drop in performance caused by the low critical temperature and high irreversibilities during compression' and expansion' processes [6]. Consequently, CO_2 transcritical cycles are mainly targeted to large-capacity systems with small participation in low-capacity applications (*9.9%* in condensing units), and very low application in stand-alone systems or plug-ins, where hydrocarbons, HFCs or HFOs are preferred for simplicity [7].

A simple solution for increasing the CO_2 critical temperature involves mixing CO_2 with small quantities of other refrigerants taking into account the restrictions of low-GWP and low (or null) flammability. The result is a zeotropic mixture with a higher critical point, lower triple-point, and lower working pressures that extend the subcritical operation of pure CO_2, minimising the irreversibilities during the transcritical process [6]. This idea, first applied by Kim & Kim [8] and Di Nicola *et al.* [9] in auto-cascades and cascades systems, respectively, was later extended to other applications to enhance their performance. Thus, in the last twenty years, different authors analysed theoretically and experimentally diverse CO_2-based blends using HFCs, HFOs and hydrocarbons in heat pumps, air conditioning and refrigeration systems. Niu & Zhang [10] tested experimentally a cascade system with the mixture CO_2/R290 (71/29%$_m$) replacing R13 in the low-temperature circuit using an internal heat exchanger (IHX) on it. The results at −65 °C demonstrate that the mixture increases the coefficient of performance (COP) by *34.2%* regarding R13 with higher cooling capacity (*39.0%*). Kim *et al.* [11] also proved experimentally, in an air conditioning system with IHX, that the mixture CO_2/R290 (75/25%$_w$) performs *12.8%* better than pure CO_2 with a significant decrement in the cooling capacity of *22.7%*. Dai *et al.* [12] analysed theoretically different

* Corresponding author.
E-mail address: sanchezd@uji.es (D. Sánchez).

https://doi.org/10.1016/j.applthermaleng.2023.121473
Received 9 June 2023; Received in revised form 9 August 2023; Accepted 31 August 2023
Available online 1 September 2023

Nomenclature

COP	Coefficient Of Performance
c_P	isobaric specific heat ($kJ \cdot kg^{-1} \cdot K^{-1}$)
G	glide (K)
GWP	Global Warming Potential (100 years)
h	specific enthalpy ($kJ \cdot kg^{-1}$)
HC	HydroCarbon
HFC	HydroFluoroCarbon
HFO	HydroFluoroOlefin
IHX	Internal Heat Exchanger
LFL	Lower Flammability Limit (%)
LMTD	Logarithmic Mean Temperature Difference (K)
$\dot{m}$	mass flow rate ($kg \cdot s^{-1}$)
N	compressor rotation speed (rpm)
NBP	Normal Boiling Point (°C)
P	pressure (bar)
$\dot{Q}$	heat transfer rate (W)
RH	Relative Humidity (%)
s	specific entropy ($kJ \cdot kg^{-1} \cdot K^{-1}$)
SH	SuperHeating (K)
T	temperature (°C)
UFL	Upper Flammability Level (%)
v	specific volume ($m^3 \cdot kg^{-1}$)
V	compressor cubic capacity (cm^3)
VCC	Volumetric Cooling Capacity ($kJ \cdot m^{-3}$)
$\dot{W}$	compressor power consumption (W)
X	it refers to the analysed parameter

Greek Symbols

Δ	variation (increment or decrement)
ε	thermal effectiveness (%)
λ	latent heat ($kJ \cdot kg^{-1}$)
η	efficiency (%)

Subscripts

amb	ambient
c	compressor
con	condenser
crit	critical point
dis	discharge
ev	evaporator
exp	expansion
G	geometric / global
gc	gas-cooler
glyc	it refers to water–ethylene–glycol mixture
hp	high-pressure
ihx	internal heat exchanger
in	inlet
int	it refers to the water–ethylene–glycol mixture at the refrigerant saturated vapour
iso	isentropic
ls	saturated liquid
m	it refers to the molar weight
max	maximum
opt	optimum
out	out
ref	it refers to the refrigerant
sf	secondary fluid
suc	suction port
V	volumetric
vs	saturated vapour
w	it refers to the mass weight

CO_2-blends with hydrocarbons, HFCs and HFOs for a single-stage without an IHX heat pump water heater, resulting in COP increments of *4.0%* and *4.5%*, using the mixtures CO_2/R41 (40/60%$_w$) and CO_2/R32 (80/20%$_w$), respectively. Bouteiller *et al.* [13,14] measured slight increases in performance using the blends CO_2/R290 (85/15%$_m$) and CO_2/R1234yf (94.5/5.5%$_m$) in central heating using an IHX. Wang *et al.* [15] computationally predict the convenience of using CO_2/R41 (50/50%$_w$) in a single-stage without an IHX heat pump water heater with COP and cooling capacity increments of *20.5%* and *25.7%*, respectively. Tobaly et *al.* [16] tested different mass fractions of CO_2/R290 in an air-conditioning and refrigeration system with IHX, obtaining COP improvements up to *19.7%* with cooling capacity decrements to *18.0%*. Yu *et al.* [17,18] experimentally analysed a mobile air conditioning with IHX using different mass fractions of CO_2/R290 and CO_2/R41, resulting in a maximum COP of *22.1%* and *25.7%*, respectively. Massuchetto *et al.* [19] studied different CO_2 blends with hydrocarbons and ammonia in a cascade cycle without IHX in the low-temperature circuit. Optimising the CO_2 mass fraction, they showed that the COP of the cascade could be enhanced by *31.0%* using a CO_2/RE170 mixture. Sun *et al.* [20] experienced heat pump water for heating and cooling with the binary blend CO_2/R32 using different R32 mass fractions. The results using a single-stage cycle with IHX showed a COP increment for heating and cooling with reductions in both capacities. Sánchez *et al.* [21] evaluated the energy consumption of a vertical beverage cooler using the blends of CO_2/R32 (78/22%$_w$) and CO_2/R1270 (92.5/7.5%$_w$) as drop-ins of pure CO_2. Using a single-stage cycle with IHX at class III environmental conditions (25)°C), the results provided energy savings of *16.5%* with CO_2/R32 and *15.5%* with CO_2/R1270. Vaccaro *et al.* [22] developed a computational model for different arrangements for CO_2, including IHX, flash-gas and ejector, using diverse CO_2-blends with hydrocarbons and HFOs. The results revealed that CO_2/R1234yf and CO_2/R290 were the best alternatives, with COP increments up to *12.8%* and *7.9%*, respectively. Similarly, Martínez-Ángeles *et al.* [23] computed the arrangements of IHX and parallel compressor with the CO_2 mixtures of R152a, R1234yf, R1234ze(E) and R1233zd(E) reaching increments up to *5.8%* using IHX and *10.0%* with the parallel compressor. Recently, Sánchez *et al.* [24] presented a theoretical analysis with five CO_2 mixtures, searching for maximising the COP without penalising the compressor capacity. The best results were reached by binary mixtures of CO_2/R32 (81/19%$_w$) and CO_2/R1270 (92.5/7.5%$_w$), with maximum COP increments of *21.4%* and *8.7%*.

Therefore, mixing CO_2 with other refrigerants results in an easy way to raise the performance of CO_2 transcritical cycles with apparent capacity reductions in heating and cooling. However, this issue can be easily fixed using the IHX, enhancing at the same time the COP. According to Torrella *et al.* [25], the IHX combined with CO_2 enhances the COP and the cooling capacity to *13.0%* and *12.0%*, respectively, especially at high heat rejection temperatures and low evaporation levels. However, to the author's knowledge, no scientific experimental studies have been published about using the IHX with CO_2 blends.

Considering this background, the present work experimentally analyses the effects of using an IHX in a CO_2 transcritical refrigerating plant upgraded with three CO_2-binary mixtures previously optimized theoretically: CO_2/R32, CO_2/R1270 and CO_2/R1234yf. Tests were performed maintaining the heat-rejecting conditions to class III (25 °C) and a constant inlet temperature of 0 °C in the evaporator for the secondary fluid, resulting in medium-temperature conditions typically used in commercial refrigeration. The results revealed the convenience of using IHX with mixtures providing increments up to *22.2%* in COP at the mentioned conditions compared to pure CO_2 without IHX.

2. Theoretical analysis

This section determines blends' optimal CO_2 mass fraction using a computational model developed and validated with experimental data. The expected results obtained will be proved experimentally in Section 3.

2.1. Cycle and mixture selection

The refrigeration cycle used for the theoretical analysis corresponds to a single-stage transcritical vapour compression cycle equipped with an IHX and an expansion system controlling the useful superheating at the evaporator outlet (Fig. 1).

Regarding the CO_2 mixtures used in this work, the previous work presented by Sánchez et al. [21] demonstrated the convenience of using blends of CO_2 with R32 and R1270 for energy savings in a vertical beverage cooler. Moreover, Vaccaro *et al.* [22] and Sánchez *et al.* [24] analysed the COP benefits of mixing CO_2 with R1234yf to replace pure CO_2 in a transcritical refrigerating plant. Therefore, the CO_2/R32, CO_2/R1270 and CO_2/R1234yf have been selected to explore the benefits of using them as potential *drop-ins* in a CO_2 transcritical refrigerating plant.

The main properties of the mixture fluids are summarised in Table 1, where NBP is the normal boiling point, P_{crit} and T_{crit} are the pressure and temperature at the critical point, and LFL and UFL are the lower and upper flammability limits taken from Calm [26] and Honeywell [27]. The values of GWP are referred to 100 years and were taken from the IPCC 6th Assessment Report [28] and Hodnebrog *et al.* [29], while the safety group classification is defined by ASHRAE Standard 34 [30].

The following criteria are considered to determine the optimal CO_2 mass fraction in each binary mixture: a) GWP_{100} lower than 150, b) non-flammable conditions, and c) maximum COP without significant cooling capacity reduction using the same compressor capacity.

The GWP requirement was described by Agarwal & Clark [31], considering that the GWP of the refrigerant blend is the mass-weighted average of GWPs of individual components in the mixture.

The non-flammability conditions were defined using the Fuel Inertization Point defined by Kondo et *al.* [32], where the minimum amount of CO_2 for flammability suppression depends on the upper and lower flammability levels.

Table 2 presents the theoretical minimum CO_2 mass fraction to guarantee a theoretical non-flammability and a GWP_{100} below 150. Notwithstanding, it is important to highlight that the previous calculation does not consider fractionation analysis due to leakage. Therefore, the CO_2 mass fractions in Table 2 should increase in case of leakage.

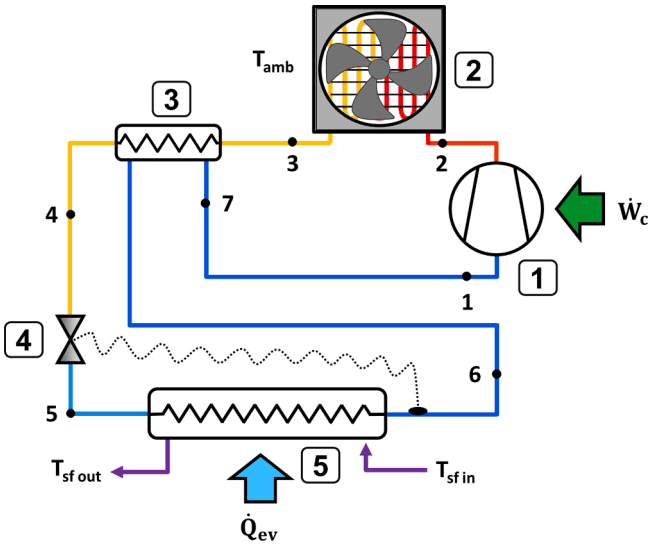

Fig. 1. Schematic diagram of the refrigeration cycle: (1) compressor, (2) gas-cooler or condenser, (3) IHX, (4) thermostatic expansion valve, (5) evaporator.

Concerning the maximum COP requirement, Section 2.2 describes the mathematical model used to determine the refrigerant mass fraction that maximises the COP of the cycle depicted in Fig. 1, considering the maximum refrigerant mass fraction shown in Table 2.

2.2. Computational model

The computational model is based on mass and energy conservation principles with no pressure drop inside the pipelines and heat exchangers. Thermophysical properties of mixtures are evaluated with the software RefProp v.10.0, which estimates the properties of mixtures by using mixing rules with a series of interaction parameters adjusted from experimental or theoretical simulations data [33,34].

Table 3 contains the model input data used for all mixtures. These values were obtained from the experimental analysis performed in Section 4 with pure CO_2 and are assumed the same for all examined mixtures in the first approach.

To determine the maximum COP for each mixture, the model varies the refrigerant mass fraction and the heat rejection pressure (P_{hp}). The first is limited by the values presented in Table 2, and the second depends on the temperature at the exit of the condenser/ gas-cooler (T_3) defined by Eq. (1).

$$T_3 = T_{amb} + \Delta T_{amb} \tag{1}$$

If T_3 is lower than the mixture's critical temperature, the heat rejection pressure varies from the condensing level to a maximum of 100 bar. Otherwise, the pressure varies from the critical pressure to 100 bar.

Due to the zeotropic behaviour of the mixture, the evaporating process is defined using the logarithmic mean temperature difference ($LMTD_{ev}$) (Eq. (2), where the useful superheating is neglected for an easy convergence of the model. This equation involves the secondary fluid temperatures ($T_{sf\ in}$ and $T_{sf\ out}$), the evaporator's inlet temperature (T_5), and the evaporator's outlet temperature in saturated conditions (T_{vs}).

$$LMTD_{ev} = \frac{(T_{sf\ in} - T_{vs}) - (T_{sf\ out} - T_5)}{\ln\left(\frac{T_{sf\ in} - T_{vs}}{T_{sf\ out} - T_5}\right)} \tag{2}$$

Fixing the $LMTD_{ev}$, Eq. (2) has two unknown's parameters (T_5 and T_{vs}) that share the same evaporating pressure level. Temperature T_5 depends on the enthalpy h_5 and the evaporating pressure (P_{ev}) (Eq. (3), while T_{vs} is defined in saturated vapour conditions with the evaporating pressure (Eq. (4)).

$$T_5 = f(h_5, P_{ev}) \tag{3}$$

$$T_{vs} = f(vs; P_{ev}) \tag{4}$$

Once defined the evaporating pressure, the temperature at the evaporator outlet considering useful superheating (SH_{ev}), is defined by Eq. (5).

$$T_6 = T_{vs} + SH_{ev} \tag{5}$$

Assuming isenthalpic expansion, h_5 is equal to enthalpy at the exit of the IHX (h_4), which value is determined by an energy balance in the IHX considering no heat exchanges with surroundings (Eq. (6)).

$$h_4 = h_3 - (h_7 - h_6) \tag{6}$$

Enthalpies h_3 and h_6 can be defined with equations Eq. (7) and Eq. (8), while h_7 is obtained with the IHX thermal effectiveness taking vapour as the fluid with less thermal capacity (Eq. (9)).

$$h_6 = f(T_6, P_{ev}) \tag{7}$$

Table 1
Main properties of the fluids analysed.

Name	Family	Molar mass (g·mol^{-1})	NBP (°C)	P_{crit} (bar)	T_{crit} (°C)	Safety group	LFL (%)	UFL (%)	GWP_{100}
R744 (CO_2)	Inorganic	44.0	−78.4	73.8	31.1	A1	–	–	1
R32	HFC	52.0	−51.7	57.8	78.1	A2L	133	29.3	771
R1234yf	HFO	114.0	−29.5	33.8	94.7	A2L	6.2	12.3	4
R1270	HC	42.1	−47.7	46.7	92.4	A3	2.2	11.0	2

Table 2
Minimum CO_2 mass fraction to guarantee non-flammability and GWP_{100} below 150.

Mixture	% CO_2	% Refrigerant	GWP_{100}
CO_2 / R32	80.7%$_w$	19.3%$_w$	149.6
CO_2 / R1234yf	44.6%$_w$	55.4%$_w$	2.7
CO_2 / R1270	92.4%$_w$	7.6%$_w$	1.1

Table 3
Model input data.

Variable	Description	Value
T_{amb}	Ambient temperature	25 °C
ΔT_{amb}	Approach temperature (condenser/gas-cooler)	7.1 K
V_G	Compressor cubic capacity	1.75 cm^3
N	Compressor rotation speed	2900 rpm
ε_{ihx}	IHX thermal effectiveness	0 / 58%
SH_{suc}	Non-useful superheating	6 K
$T_{sf\ in}$	Secondary fluid inlet temperature (evaporator)	0 °C
$T_{sf\ out}$	Secondary fluid outlet temperature (evaporator)	−7 °C
SH_{ev}	Useful superheating (evaporator)	6 K
$LMTD_{ev}$	Logarithmic mean temperature (evaporator)	4.5 K

$$h_3 = f(T_3, P_{hp}) \tag{8}$$

$$T_7 = T_6 + \varepsilon_{ihx}\cdot(T_3 - T_6) \tag{9}$$

Considering the set of equations from 2 to 8, the evaporating pressure level is the only unknown that can be determined by an iterative loop shown in Fig. 3, according to the input data established in Table 3.

Once the evaporating level is determined, the compressor behaviour is evaluated with the parametric model adjusted by Sánchez *et al.* [35] for pure CO_2, since no compressor models were found in literature for the analysed mixtures. This model allows obtaining the volumetric (η_V) and global efficiency (η_G) (Eqs. (10) and (11), respectively) using the empirical coefficients of Table 4.

$$\eta_V = a_0 + a_1\cdot P_{ev} + a_2\cdot P_{hp} + a_3\cdot(T_7 + SH_{suc}) \tag{10}$$

$$\eta_G = b_0 + b_1\cdot P_{ev} + b_2\cdot P_{hp} + b_3\cdot(T_7 + SH_{suc}) \tag{11}$$

The refrigerant mass flow rate ($\dot{m}$) and the compressor power consumption ($\dot{W}_c$) are computed with equations Eqs. (12) and (13), respectively, using the specific volume at the suction state (v_1) and the isentropic discharge enthalpy ($h_{2\ iso}$) defined with the entropy at the suction state (s_1).

$$\dot{m} = \frac{\eta_V\cdot V_G\cdot N}{v_1\cdot 60} \tag{12}$$

Table 4
Experimental coefficients for the CO_2 hermetic compressor.

Coefficient	η_V	Coefficient	η_G
a_0	0.8748614461	b_0	0.5228303246
a_1	0.0046715654	b_1	−0.0001637017
a_2	−0.0035665060	b_2	−0.0002120453
a_3	0.0022098618	b_3	0.0017040840

$$\dot{W}_c = \dot{m}\cdot\frac{(h_{2\,iso} - h_1)}{\eta_G} \qquad h_{2\,iso} = f(s_1; P_{hp}) \tag{13}$$

Finally, the cooling capacity ($\dot{Q}_{ev}$) and the coefficient of performance (COP) are obtained with equations Eqs. (14) and (15), respectively.

$$\dot{Q}_{ev} = \dot{m}\cdot(h_6 - h_5) \tag{14}$$

$$COP = \frac{\dot{Q}_{ev}}{\dot{W}_c} \tag{15}$$

The process described above is repeated, varying the refrigerant mass fraction and the heat rejection pressure until finding the optimal heat rejection pressure that maximises the system's COP. Fig. 2 presents a simplified flowchart of the computational model, including the two loops used for finding the evaporating pressure and the optimal heat rejection pressure.

2.3. Model validation

The developed model has been validated with the experimental data presented in Section 4 using pure CO_2. This data includes 13 tests with and without IHX at the ambient temperature of 25 °C, maintaining the evaporator inlet temperature for the secondary fluid to 0 °C and a useful superheating of 6 K. Fig. 3 compares the cooling capacity and the power

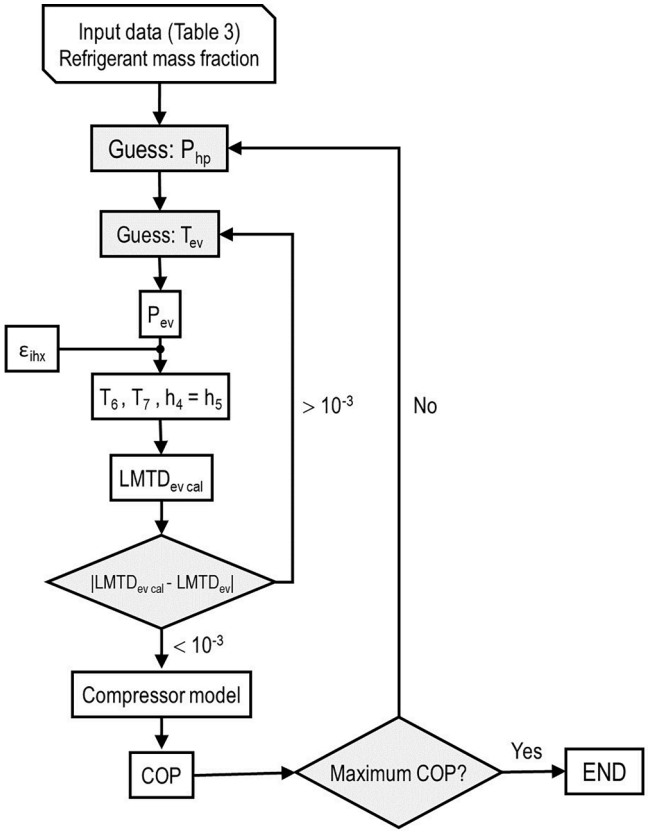

Fig. 2. Flowchart of the computational model.

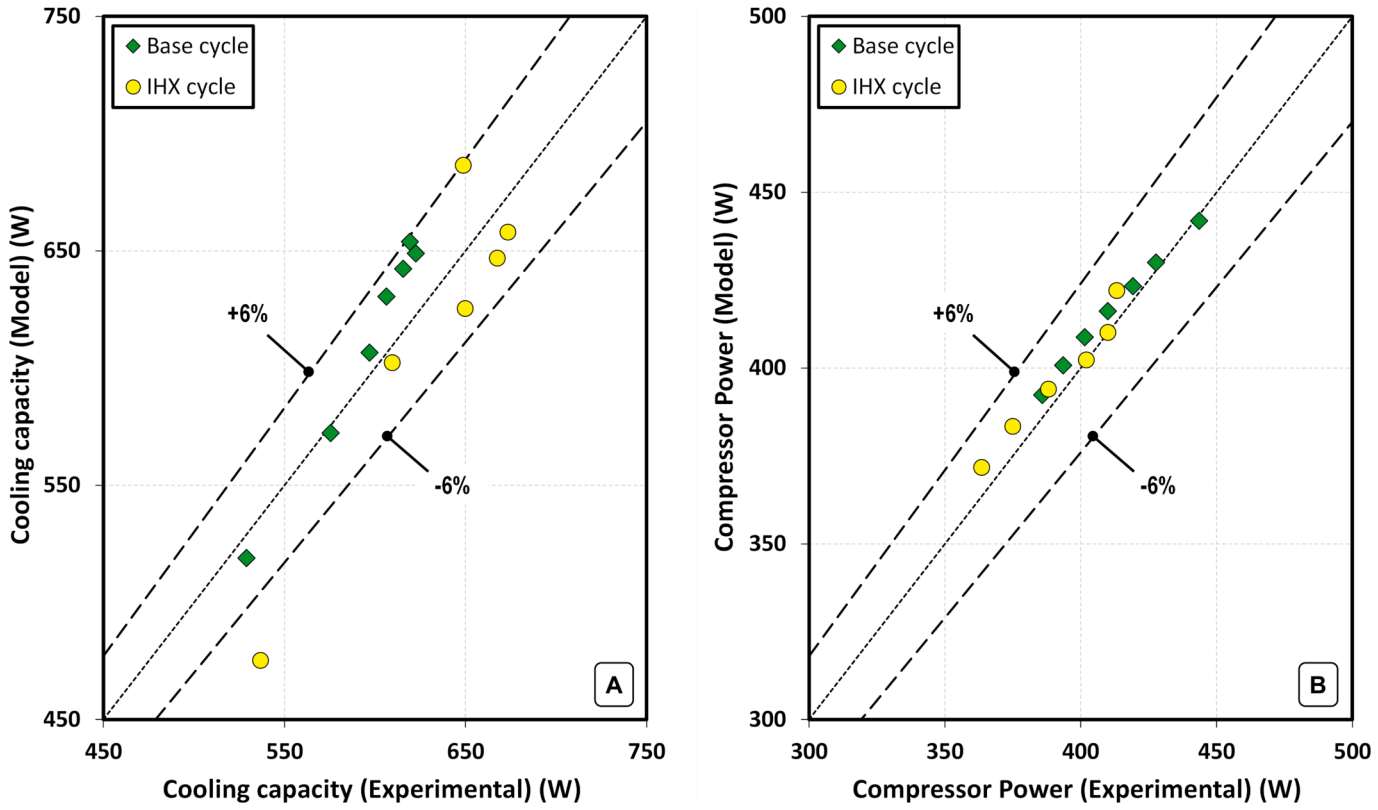

Fig. 3. Computational model validation with CO_2 using the cooling capacity (A) and the compressor power consumption (B).

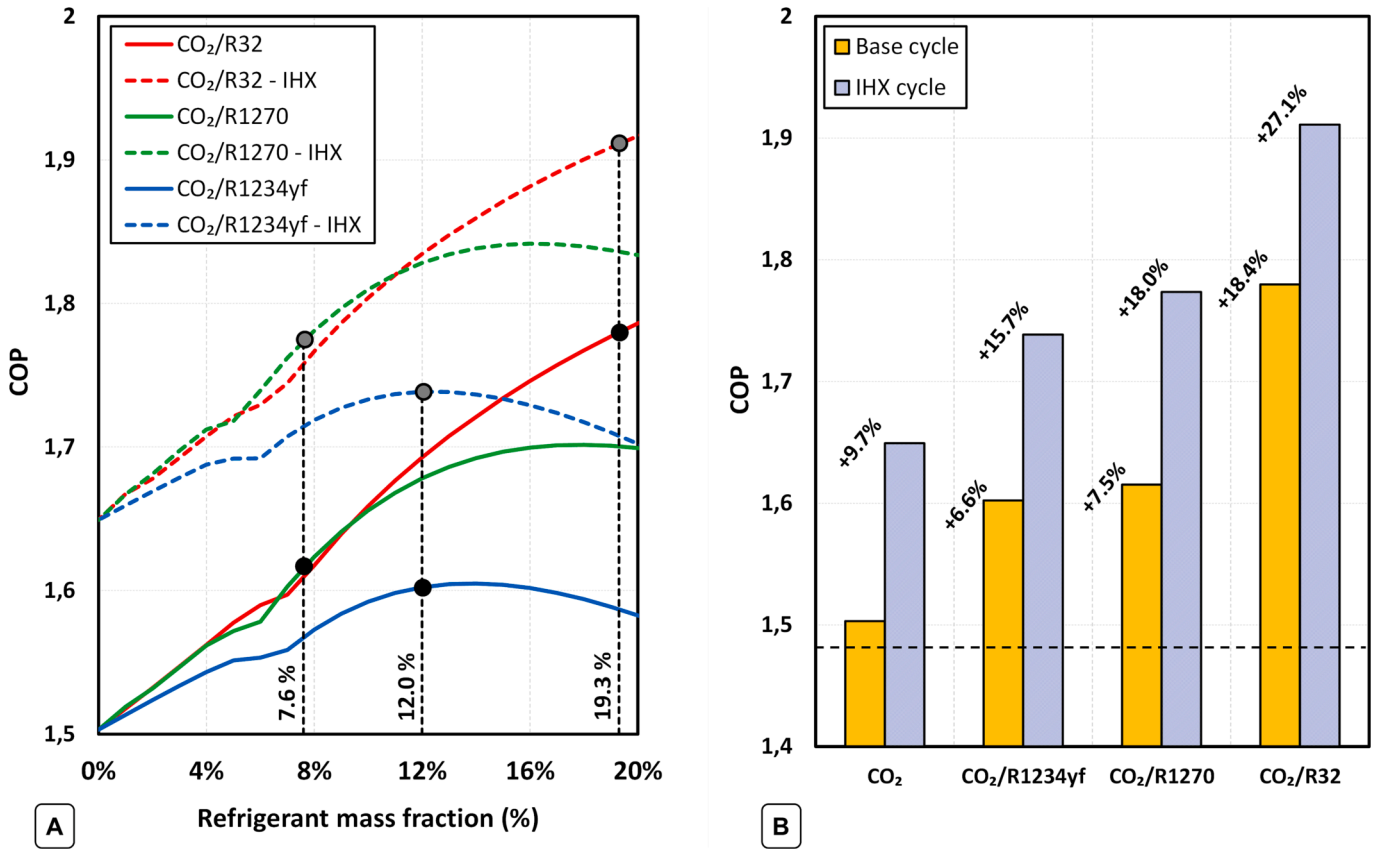

Fig. 4. Optimal COP variation with the refrigerant mass fraction (A) and COP values at the fractions of 7.6%$_w$ (R1270), 12%$_w$ (R1234yf) and 19.3%$_w$ (R32) (B).

consumption calculated from the developed model and the experimental data. As it can appreciate, the model predicts the energy parameters inside the error range of ± 6% with a maximum deviation of *11.5%* in cooling capacity near the critical point. Since this operation pressure is far from the optimal working point (maximum COP), it corresponds to a non-usual working condition and can be neglected. Therefore, the computational model can be assumed valid.

2.4. Model results

Using the model described above, the COP of the cycle can be calculated at any specific operating conditions. However, the most valuable conditions correspond to these in which COP is maximum. Accordingly, the model has been used to determine the heat rejection pressure that maximises the COP using CO_2 and mixtures. Fig. 4A presents the optimum COP with and without IHX as a function of the refrigerant mass fraction added to CO_2. This Figure points out the limits of Table 2 excepting R1234yf, in which mass fraction has been fixed to the optimum COP with IHX. The resulting COPs from these limits are highlighted in Fig. 4B, where it is noticed a COP enhancement with the use of mixtures and the IHX. These values are also presented in Table 5, including the energy parameters of the cooling capacity ($\dot{Q}_{ev}$) and compressor power consumption ($\dot{W}_c$) at optimal operating conditions.

Table 5 increments are determined by taking the results of CO_2 without IHX as a reference. Equations Eqs. (16) and (17) are used to determine ΔP_{opt} and the increments of $\Delta\dot{Q}_{ev}$, $\Delta\dot{W}_c$ and ΔCOP, respectively.

$$\Delta P_{opt} = P_{opt} - P_{opt\ CO_2\ without\ IHX} \tag{16}$$

$$\Delta X = \frac{(X - X_{CO_2\ without\ IHX})}{X_{CO_2\ without\ IHX}} \cdot 100 \tag{17}$$

According to Table 5 and Fig. 4B, using CO_2-based blends provides COP increments of *18.4*, *7.5* and *6.6%* when R32, R1270 and R1234yf are added to the mixture, respectively. Moreover, if the IHX is installed at the exit of the gas-cooler (Fig. 1), the improvement rises to *9.7%* with CO_2, *15.7%* with R1234yf, *18.0%* with R1270 and *27.1%* with R32, proving that the presence of the IHX is always positive regardless the mixture tested.

To explain the COP evolution is necessary to analyse the cooling capacity and the compressor power consumption. The first one lowers by *5.7%*, *6.4%*, and *9.4%*, with mixtures of CO_2/R32, CO_2/R1270 and CO_2/R1234yf, respectively, in concordance with the state of art. However, the presence of the IHX partially offsets this reduction, reaching a cooling capacity similar to that obtained with pure CO_2 without IHX. Concerning the compressor power consumption, the effect caused by mixtures reduces this value significantly to *20.4%* with CO_2/R32, *15.0%* with CO_2/R1234yf, and *12.9%* with CO_2/R1270. Moreover, the presence of the IHX also minimises this value reaching reductions of *2.5%* using CO_2, *21.6%* with CO_2/R32, *16.1%* with CO_2/R1234yf, and *14.3%* with CO_2/R1270.

Finally, mixtures reduce the optimal heat rejection value significatively, especially when mixtures operate in subcritical conditions. Thus, for CO_2/R32 the reduction is *17.4 bar*, for CO_2/R1234yf is *11.8 bar*, and for CO_2/R1270 it reaches *11.1 bar*.

2.5. Thermophysical properties of selected mixtures

Table 6 summarizes the thermophysical properties of the resulting mixtures, including critical pressure (P_{crit}) and temperature (T_{crit}); evaporating pressure (P_{ev}), latent heat (λ_{ev}), total glide (G_{ev}) and volumetric cooling capacity (VCC) at −10 °C with a vapour quality of 50%; specific volume ($v_{ev\ vs}$) at saturated vapour conditions; and the condensing properties of pressure (P_{con}), latent heat (λ_{con}) and total glide (G_{con}) at 30 °C with a vapour quality of 50%. Fig. 5 presents the pressure enthalpy diagram of all mixtures including pure CO_2.

According to Table 6, all alternative blends have a critical temperature and pressure higher than CO_2, extending the subcritical operation of the plant and reducing its working pressures, as can be noticed at the evaporating level and especially at the condensing level. The increments of critical temperature vary from *10.8 K* by adding 19.3% of R32 to *6.0 K* mixing with 7.6% of R1270. The effect on working pressures significantly reduces condensing pressure from *13.8 bar* with R32 to *6.6 bar* with R1270.

Concerning latent heat, mixtures increase the specific energy phase-change during the condensing and evaporating, with a significant increment in condensing (up to *152.8%* with R32) due to the extension of the subcritical operation. The benefit on the evaporating side introduces a maximum increment of *10.0%* by adding R32. However, mixtures reduce the plant's volumetric cooling capacity, defined as the ratio between the evaporation latent heat and the specific volume at the saturated vapour conditions. This parameter means the energy that the compressor moves per unit of compressor capacity, so the result of using mixtures is the need for a higher compressor cubic capacity of *16.1%* with R32, *9.7%* with R1234yf and *7.9%* with R1270. Notwithstanding, this effect will depend on how the mixtures affect the volumetric compressor efficiency.

Finally, the non-azeotropic behaviour of mixtures introduces a temperature glide during the phase-change process due to the different normal boiling point of fluids. The total glide varies from *8.8 K* with R1234yf to *3.4 K* with R1270 during the evaporation process at −10 °C, and from *4.6 K* with R1234yf to *1.8 K* with R1270 in the condensing operation at 30 °C. The effect of this glide affects the heat transfer process during the phase-change, but it allows a better matching between the refrigerant and the secondary fluid [36].

3. Experimental approach

In this section, the blends computed in Section 2 are experimentally tested in a CO_2 transcritical refrigerating plant using the configurations without and with IHX. All these blends are evaluated as *drop-ins* of CO_2 by upgrading the thermostatic expansion valve configuration.

Table 5
Simulated energy parameters.

Configuration	Refrigerant	Composition	P_{opt} (bar)	$\dot{Q}_{ev}$ (W)	$\dot{W}_c$ (W)	COP_{max}	ΔP_{opt} (bar)	$\Delta\dot{Q}_{ev}$ (%)	$\Delta\dot{W}_c$ (%)	ΔCOP_{opt} (%)
without IHX	CO_2	100%$_w$	80.5	603.1	401.2	1.50	–	–	–	–
	CO_2 / R32	80.7 / 19.3%$_w$	63.1	568.7	319.5	1.78	−17.4	−5.7	−20.4	18.4
	CO_2 / R1234yf	88.0 / 12.0%$_w$	68.7	546.7	341.2	1.60	−11.8	−9.4	−15.0	6.6
	CO_2 / R1270	92.4 / 7.6%$_w$	69.4	564.4	349.5	1.62	−11.1	−6.4	−12.9	7.5
with IHX	CO_2	100%$_w$	79.7	645.4	391.3	1.65	−0.8	7.0	−2.5	9.7
	CO_2 / R32	80.7 / 19.3%$_w$	63.1	601.3	314.7	1.91	−17.4	−0.3	−21.6	27.1
	CO_2 / R1234yf	88.0 / 12.0%$_w$	68.7	584.9	336.5	1.74	−11.8	−3.0	−16.1	15.7
	CO_2 / R1270	92.4 / 7.6%$_w$	69.4	609.5	343.7	1.77	−11.1	1.1	−14.3	18.0

Table 6
Thermophysical properties of pure CO_2 and selected CO_2-based mixtures (% in mass).

Refrigerant	Composition	P_{crit} (bar)	T_{crit} (°C)	P_{ev} (bar)	λ_{ev} (kJ·kg^{-1})	G_{ev} (K)	$v_{ev\ vs}$ (m^3·kg^{-1})	VCC (kJ/m^3)	P_{con} (bar)	λ_{con} (kJ·kg^{-1})	G_{con} (K)
CO_2	100%$_w$	73.8	31.0	26.5	258.6	0.0	0.01405	18409.7	72.1	60.6	0.0
CO_2 / R32	80.7 / 19.3%$_w$	75.8	41.8	21.1	284.5	7.5	0.01842	15447.1	58.3	153.2	4.0
CO_2 / R1234yf	88.0 / 12.0%$_w$	78.6	39.7	23.8	259.5	8.8	0.01561	16626.7	63.9	127.4	4.6
CO_2 / R1270	92.4 / 7.6%$_w$	76.2	37.0	24.4	269.2	3.4	0.01585	16952.8	65.5	117.6	1.8

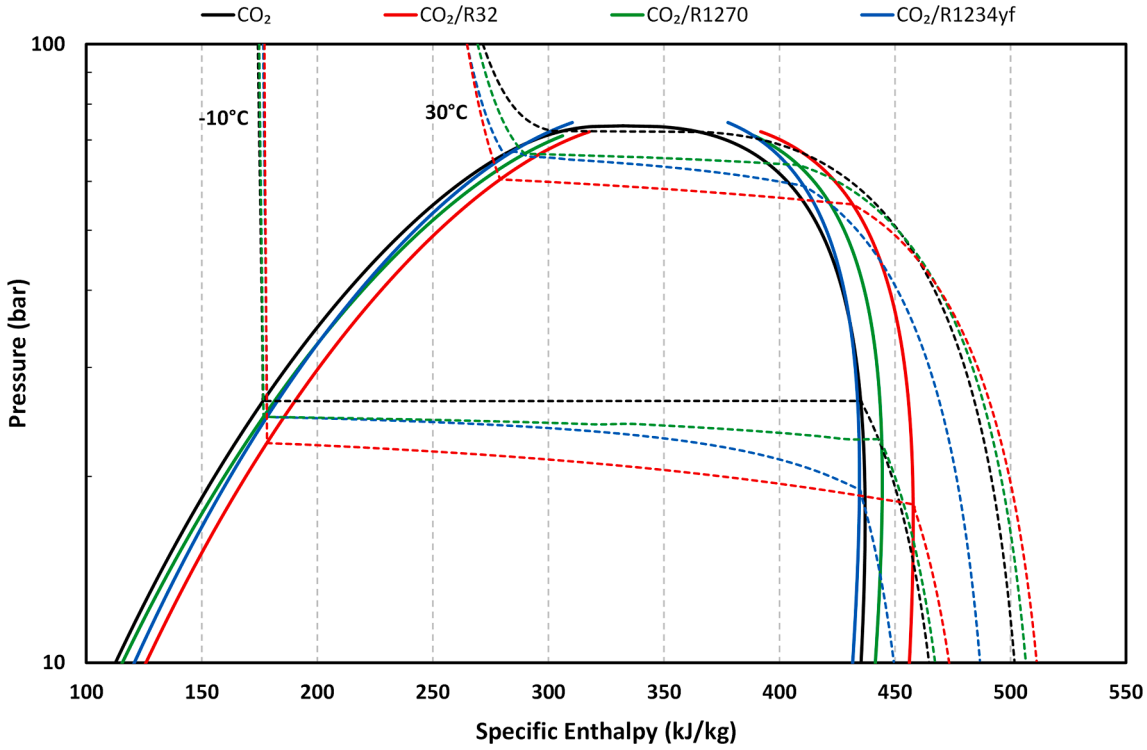

Fig. 5. Ph diagram for CO_2, CO_2/R32 (80.7/19.3%$_w$), CO_2/R1270 (92.4/7.6%$_w$) and CO_2/R1234yf (88/12%$_w$).

3.1. Refrigeration test bench

The refrigeration facility used in the experimental analysis is a low-capacity plant with a two-stage expansion system to control the useful superheating at the evaporator and the heat rejection pressure in the condenser/gas-cooler. The setup uses air as secondary fluid in the condenser/gas-cooler and a mixture of water and ethylene–glycol (49% in mass) in the evaporator. The schematic diagram of the plant is depicted in Fig. 6, including the measurement elements used to register data.

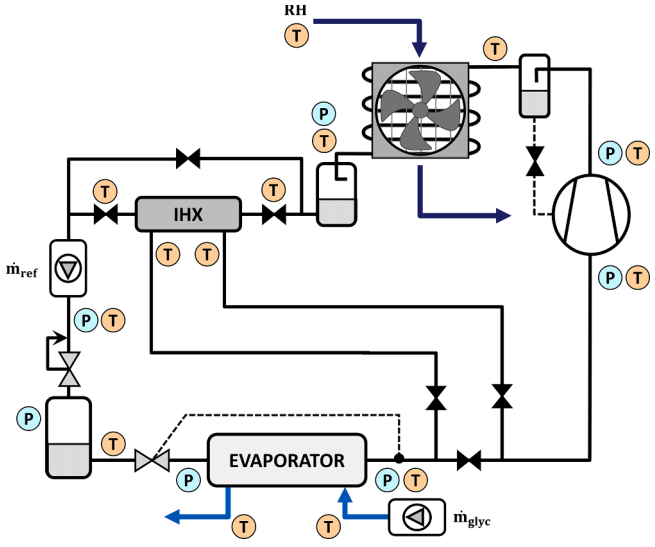

Fig. 6. Experimental test bench.

The test bench includes a hermetic compressor with a cubic capacity of 1.75 cm^3 running at a nominal speed of 2900 rpm (50 Hz); a coalescent filter installed in the discharge line to remove the PAG lubricant oil from the refrigerant stream; an air finned-tube condenser/gas-cooler with an inlet heat transfer area of 0.27 m^2 and an axial fan of 31 W to reject the heat and to cool down the compressor; a small accumulator tank of 200 cm^3; a tube-in-tube internal heat exchanger (IHX) arranged in counter-flow with two by-passes and an inner heat transfer area of 0.022 m^2; an electronic expansion valve working as back-pressure; an intermediate liquid receiver of 3700 cm^3 to ensure liquid-phase at the inlet of the thermostatic expansion valve; a second electronic expansion valve working as thermostatic controlling the superheating at the evaporator; and finally, a counter-flow brazed-plat evaporator with a heat transfer area of 0.576 m^2.

The measurement elements depicted in the Fig. 6 are summarised in the Table 7 taking into account the number of sensors, measurement range and calibrated accuracy.

In the test ring, except the discharge line, all the pipelines were insulated with a low-thermal conductivity foam to reduce the heat transfer to the environment, especially the place for the measurement

Table 7
Characteristics of the measurement elements.

Number	Measurement device	Measured Variable	Measurement range	Calibrated accuracy
13	T-type thermocouple	Temperature	−40 to 125 °C	±0.5 K
3	Pressure gauge	Pressure	0 to 160 bar	±0.6% of spam (±0.96 bar)
1	Pressure gauge	Pressure	0 to 100 bar	±0.6% of spam (±0.60 bar)
3	Pressure gauge	Pressure	0 to 60 bar	±0.6% of spam (±0.36 bar)
1	Coriolis mass flow meter	Refrigerant mass flow rate	0 to 0.1 kg·s^{-1}	±0.1% of reading
1	Coriolis mass flow meter	Water-ethylene–glycol mass flow rate	0 to 0.1 kg·s^{-1}	±0.1% of reading
1	Single-phase network analyser	Compressor power consumption	0 to 1250 W	±0.5% of reading
1	Humidity and temperature sensor	Ambient humidity and temperature	5 to 98% (RH) −20 to 80 °C (T)	± 2% (RH) ± 2 K (T)

elements.

All data from probes are acquired by a data acquisition system every 5 s for 20 min, maintaining the desired working conditions explained in section 3.2.

3.2. Test methodology

The conditions used to compare CO_2 blends were fixed by the secondary fluids of air and water-ethylene–glycol mixture at the condenser/gas-cooler and evaporator, respectively. Thus, in the condenser/gas-cooler, the air conditions were fixed to climatic class III: 25 °C and 60% of RH (UNE-EN ISO 23953–2), using a climatic chamber. At the same time, the water-ethylene–glycol mixture in the evaporator was set to 0 °C with a constant mass flow rate of 100 kg·h^{-1} using an auxiliary loop.

The heat rejection pressure was varied from 95 bar to a minimum value defined by the refrigerant when the back-pressure valve was fully opened. Finally, the useful superheating was set to 5.5 K by the thermostatic expansion valve, which controller was upgraded with the refrigerant P-T curve calculated using RefProp.

Mixture elaboration was done with a vessel of 13.4 L. This vessel was filled first with the refrigerant R32, R1270 or R1234yf, then with CO_2 according to the mass fraction presented in Table 6 using a precision scale with an uncertainty of ±1 g. The total mass introduced was limited to maintain fluids in vapour-phase at 25 °C, ensuring a uniform mixture. This limitation can easily determine by the volume of the vessel and the density of the saturated vapour phase at 25 °C of the corresponding mixture. Taking into account the mass introduced and the uncertainty of the scale, Table 8 shows the uncertainty in the mass composition.

Finally, the test order was CO_2, CO_2/R1270, CO_2/R32 and CO_2/R1234yf without and with IHX. After each refrigerant, the refrigerating cycle was vacuumed for 30 min to remove all the previous fluid. The mass charge introduced in each test was 1.3 kg regardless of the refrigerant tested.

Table 8
Uncertainty in the mixture composition (% in mass).

Mixture	Theoretical composition	CO_2 composition range (%$_w$)	Fluid composition range (%$_w$)
CO_2 / R32	80.7 / 19.3%$_w$	80.75–80.65	19.25–19.35
CO_2 / R1234yf	88.0 / 12.0%$_w$	88.05–87.95	11.95–12.05
CO_2 / R1270	92.4 / 7.6%$_w$	92.45–92.35	7.55–7.65

4. Experimental results

The results from the experimental tests described above are presented and discussed in this section, including the energy parameters of cooling capacity, compressor power consumption and coefficient of performance (COP). Moreover, mass flow rate, optimal heat rejection pressure, compressor efficiency and heat exchangers' behaviour are also included.

4.1. Cooling capacity

The cooling capacity of the plant ($\dot{Q}_{ev}$) can be determined by the equation Eq. (18) as a product of the refrigerant mass flow rate ($\dot{m}_{ref}$) and the enthalpy difference between the outlet and the inlet of the evaporator. However, it also can be calculated through the secondary fluid by the equation Eq. (19) as the product of the water-ethylene–glycol mass flow rate ($\dot{m}_{glyc}$), the isobaric specific heat ($c_{P\,glyc}$), and the temperature difference in the secondary fluid. The results obtained from both equations have been compared to validate the measurement system and the thermophysical property calculation from RefProp. Fig. 7 compares the results from Eqs. (18) and (19) for all tested fluids running without and with IHX. As can be seen, 92.6% of experimental data has an error below *6.0%* (63 out of 68 tests), with a maximum error of *6.9%*. Consequently, the experimental tests can be considered as valid.

$$\dot{Q}_{ev} = \dot{m}_{ref} \cdot (h_{ev\,out} - h_{ev\,in}) \tag{18}$$

$$\dot{Q}_{ev} = \dot{m}_{glyc} \cdot c_{P\,glyc} \cdot (T_{glyc\,in} - T_{glyc\,out}) \tag{19}$$

Fig. 8 compares the cooling capacity of all tested fluids as a function of the heat rejection pressure considering the operation without IHX (Fig. 8A) and with IHX (Fig. 8B). As can be noted, the cooling capacity varies, reaching a maximum depending on the heat rejection pressure due to the mass flow rate and the enthalpy difference shown in Eq. (18). This maximum will be taken as a reference to compare the capacities reached by mixtures with pure CO_2 without and with IHX. Accordingly, Fig. 8A reveals that CO_2/R1234yf cooling capacity is *1.7%* higher than pure CO_2 with a heat rejection pressure *3.5 bar* lower. CO_2/R1270 has a cooling capacity of *1.6%* lower than CO_2, with an optimum pressure of *4.2 bar* more down. Finally, CO_2/R32 provides the lowest cooling capacity with a reduction of *6.8%* regarding CO_2, and the lowest heat rejection pressure, resulting in a decrease of *21.0* bar compared to pure CO_2.

Moving to the IHX, Fig. 8B confirms the positive effect of the IHX on the cooling capacity regardless of the used mixture. Again, taking as a reference the heat rejection pressure that maximises the cooling capacity using the IHX, CO_2/R1234yf performs a cooling capacity *0.2%* lower than pure CO_2 with a heat rejection pressure *8.1 bar* lower. The mixture CO_2/R1270 has a cooling capacity of *1.1%* lower than CO_2, with a pressure reduction of *3.9 bar*. Finally, the cooling capacity reached with CO_2/R32 is *3.9%* lower than CO_2, with a decrease in the heat rejection pressure of *12.5 bar*.

Comparing the experimental results with the theoretical from Table 5, it is noted that the computational model underestimates the cooling capacity. This is mainly due to the assumptions taken in the computational model, which will be discussed in Sections 4.5 and 4.6.

4.2. Compressor power consumption and mass flow rate

According to Equation Eq. (13), the compressor power consumption depends on the mass flow rate, the global efficiency of the compressor and the isentropic compression work. Fig. 9 presents the effect of all

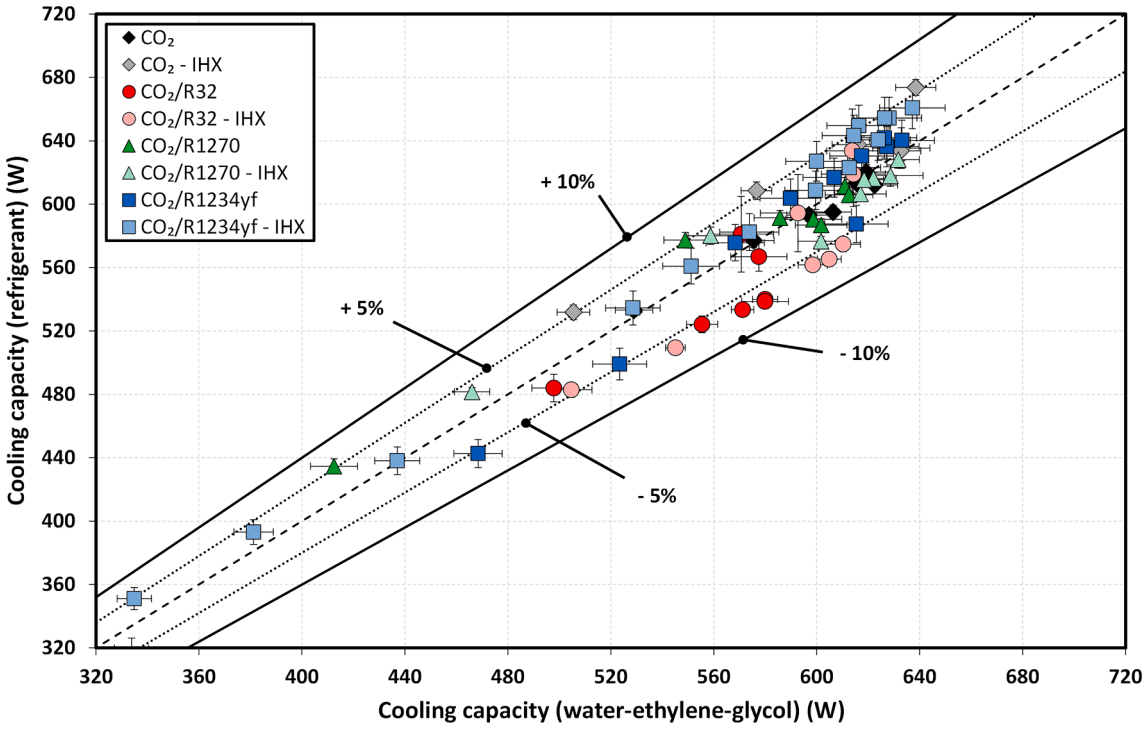

Fig. 7. Cooling capacity validation.

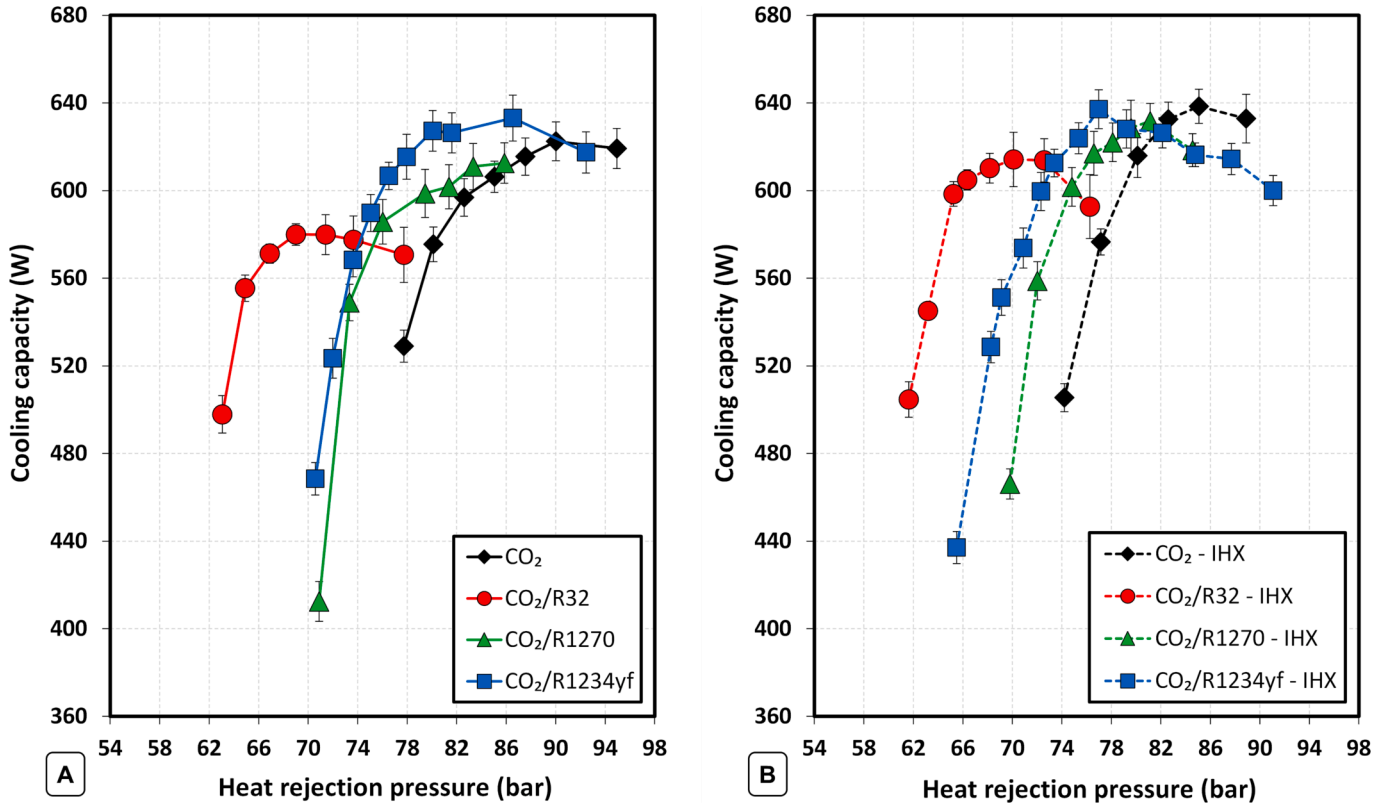

Fig. 8. Cooling capacity variation with the heat rejection pressure without IHX (A) and with IHX (B).

these parameters in both configurations: without using the IHX (Fig. 9A) and with the IHX (Fig. 9B).

As was expected in the theoretical analysis, CO_2-based mixtures reduce the compressor's power consumption due in part to the reduction that suffers the refrigerant mass flow rate driven by the compressor, which evolution with the heat rejection pressure is depicted in Fig. 10 without and with IHX.

Considering Fig. 10, CO_2 presents the highest mass flow rate, followed by CO_2/R1270, CO_2/R1234yf, and the mixture of CO_2/R32 with the lowest mass flow rate. This order is explained by equation Eq. (12),

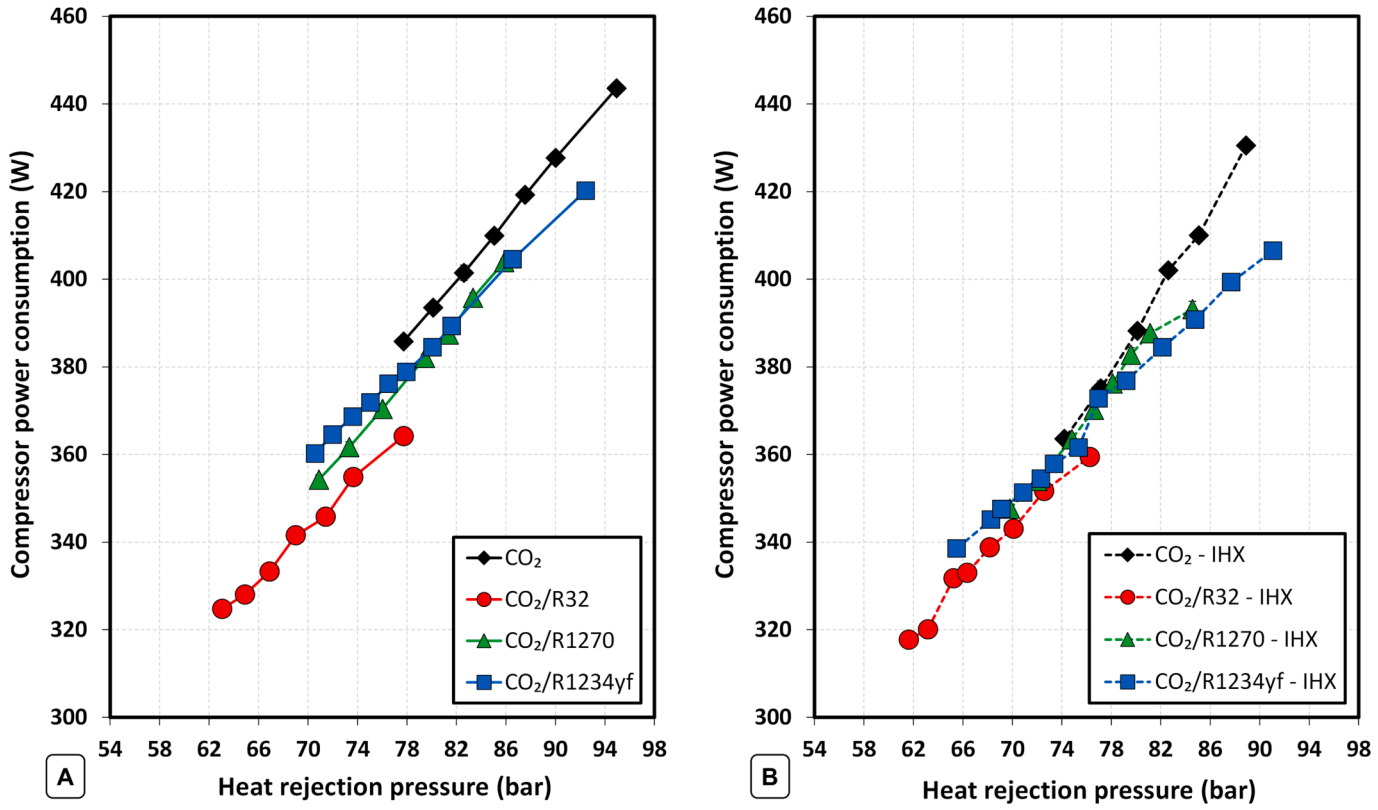

Fig. 9. Compressor power consumption vs heat rejection pressure without IHX (A) and with IHX (B).

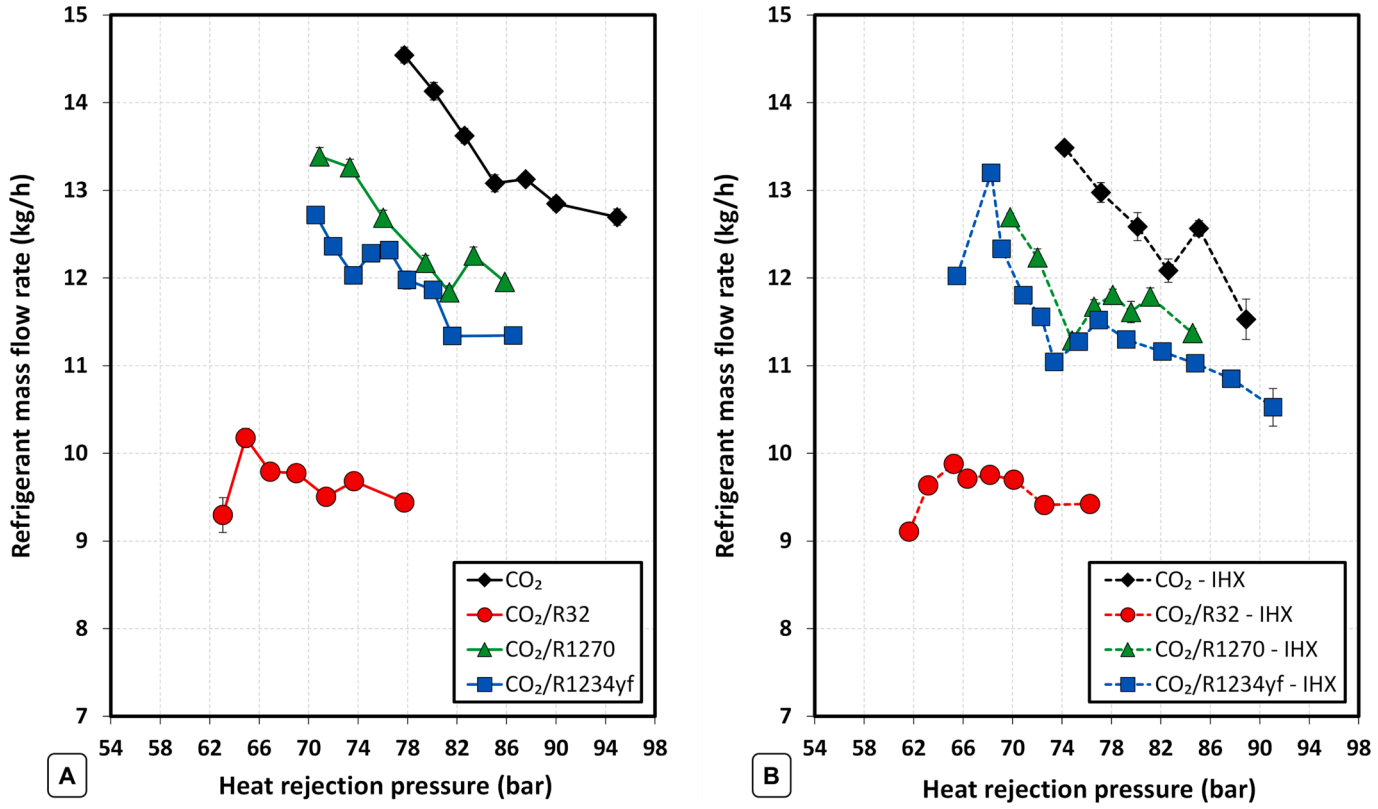

Fig. 10. Refrigerant mass flow rate vs heat rejection pressure without IHX (A) and with IHX (B).

where the mass flow rate is proportionally inverse to the specific volume. Thus, the highest specific volume (Table 6), the lowest mass flow rate (Fig. 10), and the lowest compressor power consumption (Fig. 9). The effect of the volumetric efficiency included in equation Eq. (12) will be discussed later in Section 4.6.

Finally, it is important to notice that the effect of the IHX reduces the mass flow rate and the compressor power consumption in almost all cases, except CO_2/R32, where the mass flow rate and the power consumption remain similar without and with the IHX.

4.3. Coefficient of performance and optimal heat rejection pressure

The Coefficient of Performance (COP) of a refrigerating plant represents the ratio of the useful cooling capacity and the power required to produce it. This parameter is defined by the equation Eq. (15) as the quotient between the cooling capacity analysed in Section 4.1 and the power consumed by the compressor presented in Section 4.2. Since the COP in a CO_2 transcritical system mainly depends on the heat rejection temperature, the evaporating level, and the heat rejection pressure [37], Fig. 11 presents the COP as a function of the heat rejection pressure without and with IHX (Fig. 11A and 11B, respectively).

Due to the shape of the isotherm's lines near the critical point (Fig. 4), COP curves depicted in Fig. 11 reach a maximum named "optimal COP" at a heat rejection pressure known as "optimal pressure" (P_{opt}). This optimal pressure is highlighted in Fig. 11 with a yellow star-shaped marker.

The results of maximum COP and optimal heat rejection pressure are depicted in Figs. 12 and 13, respectively, including the percentage variation regarding CO_2 results without IHX.

Fig. 11 shows the positive effect of CO_2-blends in the COP of the refrigerating plant taking into account the presence of the IHX. As can be observed, CO_2-dopped blends enhance the COP and reduce the optimal heat rejection pressure, being this effect higher with the IHX. Fig. 12 presents the maximum values of COP in both configurations with

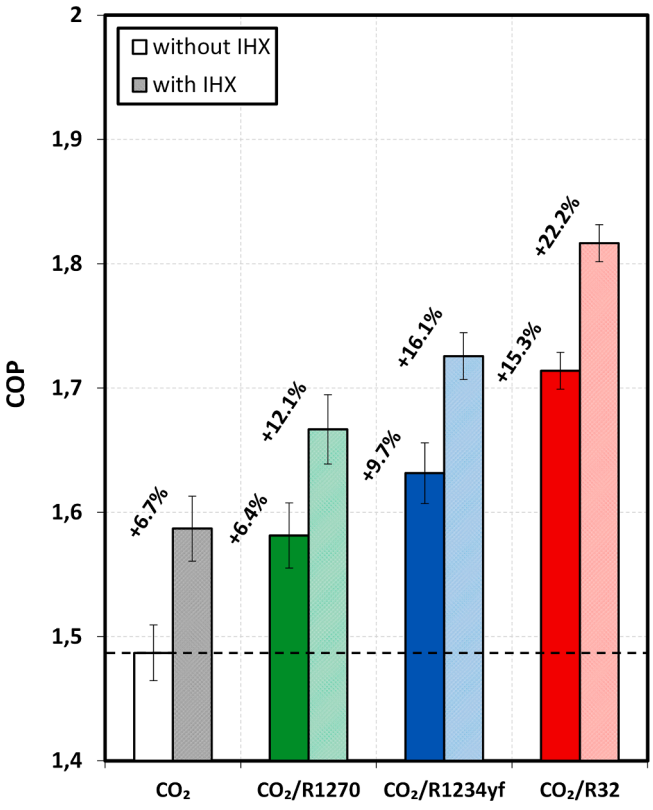

Fig. 12. Maximum cooling COP (COP_{max}).

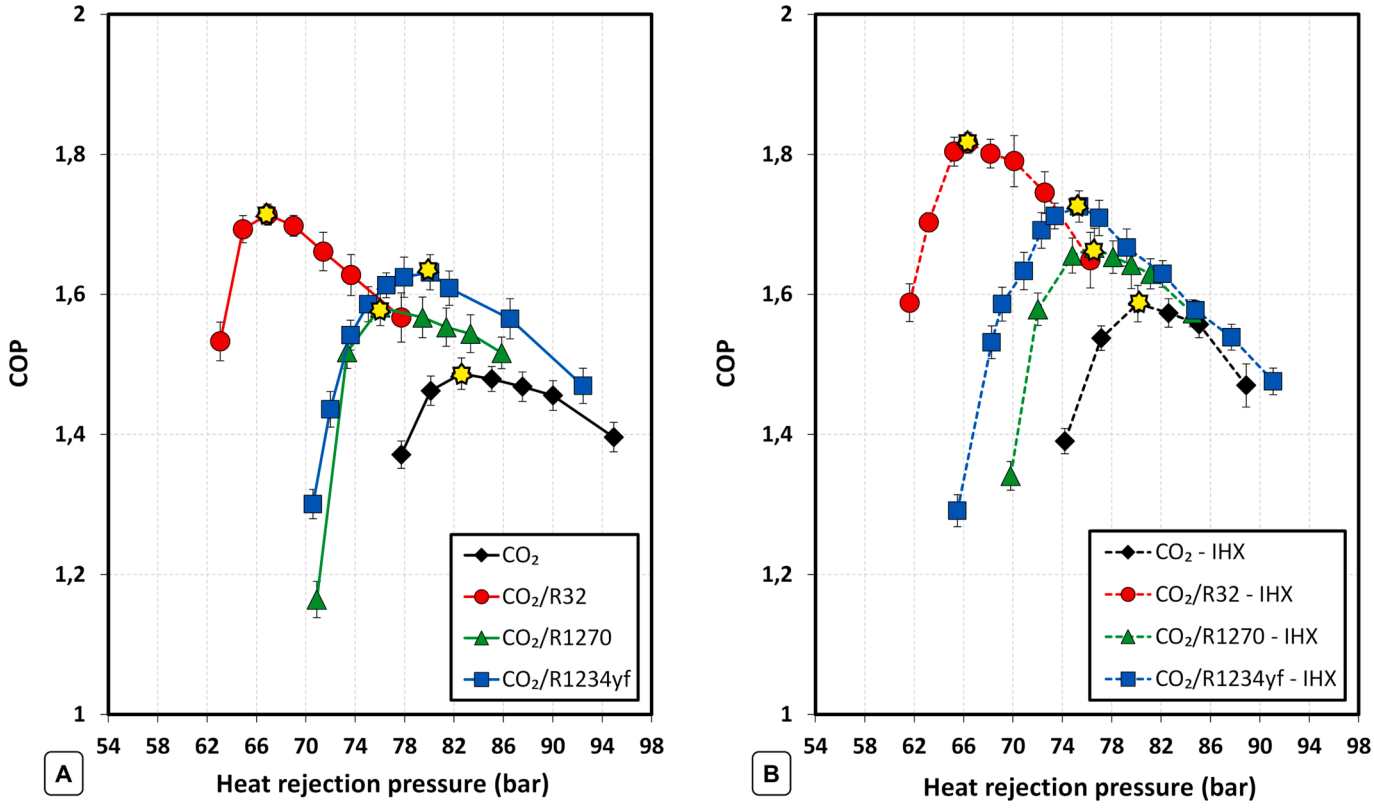

Fig. 11. COP variation with the heat rejection pressure without IHX (A) and with IHX (B).

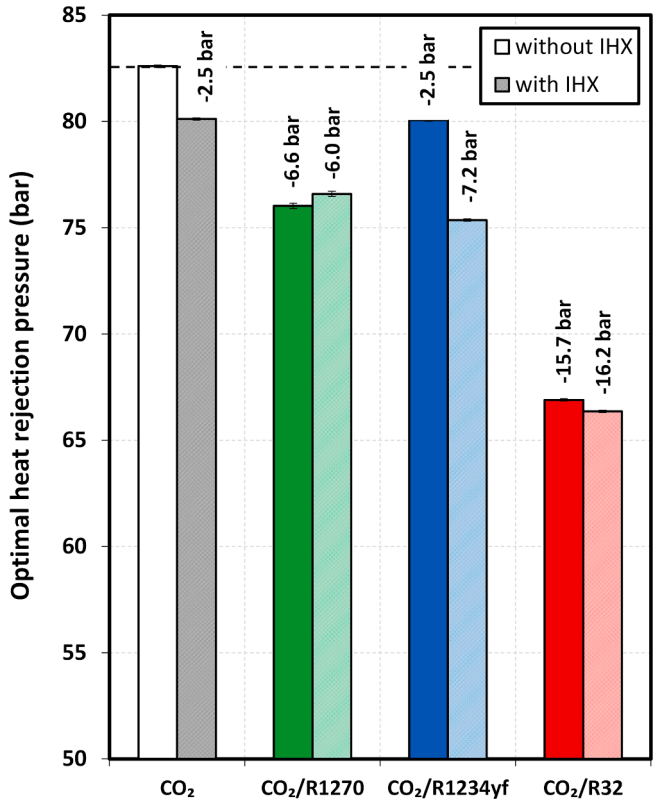

Fig. 13. Optimal heat rejection pressure (P_{opt}).

increments of *6.4%* with R1270, *9.7%* with R1234yf, and *15.3%* with R32, without IHX regarding pure CO_2. Besides that, the presence of the IHX boosts the COP in all cases resulting in *6.7%* for CO_2, *12.1%* for CO_2/R1270, *16.1%* for CO_2/R1234yf, and *22.2%* for CO_2/R32. Moreover, using mixtures always reduces the optimal heat rejection pressure from *2.5* to *16.2 bar*, according to Fig. 13. As expected, reductions of optimal pressure are higher with the presence of the IHX, following the results published by Torrella *et al.* with pure CO_2 [25].

On the other hand, comparing experimental results with the theoretical ones from Fig. 4B and Table 5, there are differences in the optimal heat rejection pressure (P_{opt}) and the maximum COP (COP_{max}). Table 9 summarizes and compares the values of P_{opt} and COP_{max}, taking the experimental data as a reference. According to Table 9, the model generally overpredicts the maximum COP in percentages from *0.7* to *6.0%*, overpredicting, at the same time, the optimal heat rejection pressure from *0.5* to *11.4 bar*.

These differences are directly connected with the assumptions taken in the computational model, which assumes the same compressor model for all fluids (Table 4) and constant values for the LMTD in the evaporator and approach temperature in the condenser/gas-cooler (Table 3). The real values of these parameters will be discussed later in Sections 4.5 and 4.6.

4.4. Working parameters at the optimal heat rejection pressure

Table 10 presents the main parameters of the refrigerating plant at the optimal heat rejection pressure shown in Fig. 13. This Table contains the reference parameters defined in Section 3.2: ambient temperature (T_{amb}) and relative humidity (RH_{amb}); water-ethylene–glycol inlet temperature ($T_{glyc\ in}$) and mass flow rate ($\dot{m}_{glyc}$); and evaporator superheating (SH_{ev}). Moreover, it includes the energy parameters of the cooling capacity ($\dot{Q}_{ev}$), compressor power consumption ($\dot{W}_c$) and COP; and other working parameters such as the evaporating temperature (T_{ev}), the condensing or gas-cooler exit temperature ($T_{con/gc}$), the optimal heat rejection pressure (P_{opt}), and the discharge temperature.

The phase-change temperatures are calculated with the mid-point temperature using the liquid and vapour-saturated temperatures in the condenser (Eq. (20) and the inlet and vapour-saturated temperatures in the evaporator (Eq. (21). In the evaporator, the inlet temperature ($T_{ev\ in}$) is determined by Eq. (22) with the evaporating inlet pressure ($P_{ev\ in}$) and the inlet enthalpy ($h_{exp\ in}$), assuming an isenthalpic expansion in the thermostatic expansion valve. This method considers the zeotropic behaviour of CO_2 mixtures and the pressure drop inside heat exchangers since saturated conditions are evaluated with the measured pressure and the software RefProp.

$$T_{con} = \frac{T_{con\ vs} + T_{con\ ls}}{2} \tag{20}$$

$$T_{ev} = \frac{T_{ev\ vs} + T_{ev\ in}}{2} \tag{21}$$

$$T_{ev\ in} = f\left(P_{ev\ in}, h_{expin}\right) \tag{22}$$

According to Table 10, CO_2 performs at the lowest evaporation level of all tested fluids, while the mixture CO_2/R1234yf conducts the highest level with, on average, *2 K* higher. Regarding CO_2/R1270, it works at an evaporating level similar to CO_2/R1234yf, while CO_2/R32 is closest to the CO_2 behaviour but, on average, *0.5 K* higher. These results mean that despite the negative effect of CO_2-blends on the evaporating heat transfer coefficient [38], the zeotropic glide offsets this effect increasing the evaporating temperature level.

Moving to gas-cooler exit temperature, excepting CO_2/R32, mixtures CO_2/R1270 and CO_2/R1234yf present lower gas-cooler exit temperatures than CO_2. Therefore, CO_2-dopped blends perform better than pure CO_2 in transcritical conditions benefiting heat recovery processes. Concerning CO_2/R32, the high critical temperature of this mixture (Table 6) yields a subcritical operation with an average condensing temperature of *5 K* higher than the CO_2 gas-cooler exit temperature.

Finally, Table 10 confirms that the IHX always increases the compressor discharge temperature with non-remarkable differences among tested fluids. Thus, for the base cycle without IHX, this temperature varies from *80.8* to *86.0* °*C*, with the maximum value reached by

Table 9
Comparison between the computational model results and the experimental tests.

Configuration	Refrigerant	Composition	MODEL		EXPERIMENTAL		Difference	
			P_{opt} (bar)	COP_{max}	P_{opt} (bar)	COP_{max}	ΔP_{opt} (bar)	ΔCOP_{max} (%)
without IHX	CO_2	100%$_w$	80.5	1.50	82.6	1.49	*2.1*	*−1.1*
	CO_2 / R32	80.7 / 19.3%$_w$	63.1	1.78	66.9	1.71	*3.8*	*−3.7*
	CO_2 / R1234yf	88.0 / 12.0%$_w$	68.7	1.60	80.1	1.63	*11.4*	*1.8*
	CO_2 / R1270	92.4 / 7.6%$_w$	69.4	1.62	76.0	1.58	*6.7*	*−2.1*
with IHX	CO_2	100%$_w$	79.7	1.65	80.1	1.59	*0.5*	*−3.8*
	CO_2 / R32	80.7 / 19.3%$_w$	63.1	1.91	66.4	1.82	*3.3*	*−4.9*
	CO_2 / R1234yf	88.0 / 12.0%$_w$	68.7	1.74	75.4	1.73	*6.7*	*−0.7*
	CO_2 / R1270	92.4 / 7.6%$_w$	69.4	1.77	76.6	1.67	*7.2*	*−6.0*

Table 10
Main parameters of the refrigerating unit at the optimal operating conditions (* means in subcritical conditions).

Refrigerant		T_{amb} (°C)	RH_{amb} (%)	$T_{glyc\ in}$ (°C)	$\dot{m}_{glyc}$(kg/s)	T_{ev} (°C)	SH_{ev} (K)	$T_{con/gc\ out}$ (°C)	T_{dis} (°C)	P_{opt} (bar)	$\dot{Q}_{ev}$(W)	$\dot{W}_c$(W)	COP_{opt}
CO_2	without IHX	25.2 ± 0.0	60.3 ± 0.4	0.0 ± 0.1	100.5 ± 0.5	−8.9 ± 0.1	5.9 ± 0.1	32.3 ± 0.1	83.2 ± 0.1	82.6 ± 0.0	596.9 ± 8.6	401.5 ± 1.8	1.49 ± 0.02
	with IHX	25.2 ± 0.1	60.3 ± 0.4	0.0 ± 0.1	100.6 ± 0.7	−9.1 ± 0.1	5.9 ± 0.2	32.3 ± 0.1	90.0 ± 0.1	80.1 ± 0.1	616.0 ± 10.0	388.2 ± 1.7	1.59 ± 0.03
CO_2 / R32	without IHX	24.8 ± 0.1	60.3 ± 0.2	−0.1 ± 0.1	99.9 ± 0.5	−8.2 ± 0.1	5.7 ± 0.1	37.6 * ± 0.1	81.6 ± 0.1	66.9 ± 0.1	571.2 ± 4.4	333.3 ± 0.9	1.71 ± 0.01
	with IHX	25.0 ± 0.1	59.1 ± 0.2	−0.1 ± 0.1	100.0 ± 0.3	−8.4 ± 0.0	5.6 ± 0.1	37.3 * ± 0.1	86.8 ± 0.1	66.4 ± 0.1	604.9 ± 4.7	333.3 ± 0.7	1.82 ± 0.01
CO_2 / R1234yf	without IHX	25.2 ± 0.1	57.8 ± 0.1	0.0 ± 0.1	99.2 ± 0.5	−6.6 ± 0.0	3.7 ± 0.1	29.9 ± 0.1	86.0 ± 0.1	80.1 ± 0.1	627.2 ± 9.2	384.5 ± 1.0	1.63 ± 0.02
	with IHX	25.1 ± 0.0	54.4 ± 0.1	0.0 ± 0.1	100.0 ± 0.5	−7.1 ± 0.0	3.3 ± 0.1	30.0 ± 0.1	88.2 ± 0.1	75.4 ± 0.1	640.5 ± 1.3	361.5 ± 1.5	1.73 ± 0.02
CO_2 / R1270	without IHX	25.1 ± 0.0	58.7 ± 0.1	0.1 ± 0.2	99.4 ± 0.7	−7.3 ± 0.1	6.2 ± 0.1	32.0 ± 0.1	80.8 ± 0.1	76.0 ± 0.1	585.8 ± 10.1	370.4 ± 1.2	1.58 ± 0.03
	with IHX	25.2 ± 0.1	56.1 ± 0.2	−0.1 ± 0.1	100.4 ± 0.5	−7.7 ± 0.1	6.1 ± 0.1	31.4 ± 0.1	88.6 ± 0.1	76.6 ± 0.1	617.0 ± 10.0	370.2 ± 1.1	1.67 ± 0.03

the CO_2/R1234yf mixture. Using the IHX, the range goes from *88.2* to *90.0* °*C*, with the maximum for CO_2 operation.

4.5. Heat exchangers performance

The performance of the heat exchangers used in the refrigeration plant can be determined by using the parameters of logarithmic mean temperature difference ($LMTD_{ev}$) and thermal effectiveness (ε_{ev}) in the evaporator, the approach temperature (ΔT_{amb}) in the condenser/gas-cooler, and the thermal effectiveness (ε_{ihx}) in the IHX.

The $LMTD_{ev}$ is determined using equation Eq. (23), considering evaporator inlets and outlets from refrigerant and secondary fluid in the evaporator's phase-change region. Accordingly, the water-ethylene–glycol intermediate temperature ($T_{glyc\ int}$) in Eq. (23) is determined using the heat transfer balance in Eq. (24).

$$LMTD_{ev} = \frac{\left(T_{glyc\ int} - T_{ev\ vs}\right) - \left(T_{glyc\ out} - T_{ev\ in}\right)}{\ln\left(\frac{T_{glyc\ int} - T_{ev\ vs}}{T_{glyc\ out} - T_{ev\ in}}\right)} \tag{23}$$

$$T_{glyc\ int} = T_{glyc\ out} + \frac{\dot{m}_{ref} \cdot \left(h_{ev\ vs} - h_{ev\ in}\right)}{\dot{m}_{glyc} \cdot c_{Pglyc}} \tag{24}$$

The ε_{ev} is obtained with equation Eq. (25), considering the water-glycol mixture as the fluid with less thermal capacity. As the $LMTD_{ev}$, the thermal effectiveness only considers the evaporator's phase-change region.

$$\varepsilon_{ev} = \frac{T_{glyc\ int} - T_{glyc\ out}}{T_{glyc\ int} - T_{ev\ in}} \tag{25}$$

The approach temperature (ΔT_{amb}) is calculated with equation Eq. (26), and it is the difference between the temperature at the condenser/gas-cooler outlet and the ambient temperature.

$$\Delta T_{amb} = T_{con/gc\ out} - T_{amb} \tag{26}$$

Finally, the IHX thermal effectiveness (ε_{ihx}) is obtained using Eq. (27), considering the vapour from evaporator outlet as the fluid with less thermal capacity.

$$\varepsilon_{ihx} = \frac{T_{ihx\ lp\ out} - T_{ihx\ lp\ in}}{T_{con/gc\ out} - T_{ihx\ lp\ in}} \tag{27}$$

Results from expressions (23) and (25) are depicted in Figs. 14 and 15, respectively, as a function of the pressure ratio defined by the ratio between the pressure at the discharge and suction port. Regardless the IHX, Fig. 14 shows that LMTD values are higher for CO_2 and CO_2/R32 (*4* to *5 K*) than CO_2/R1270 and CO_2/R1234yf (*2* to *3.5 K*). These results explain the highest evaporating temperature for mixtures with R1270 and R1234yf, presented in Table 10. Nonetheless, a lower LMTD does not mean higher thermal effectiveness, as Fig. 15 shows. Accordingly, CO_2 and CO_2/R1270 reach the highest values of ε_{ev} (almost *80%*), followed by CO_2/R1234yf and CO_2/R32 with *65%* and *56%* on average, respectively.

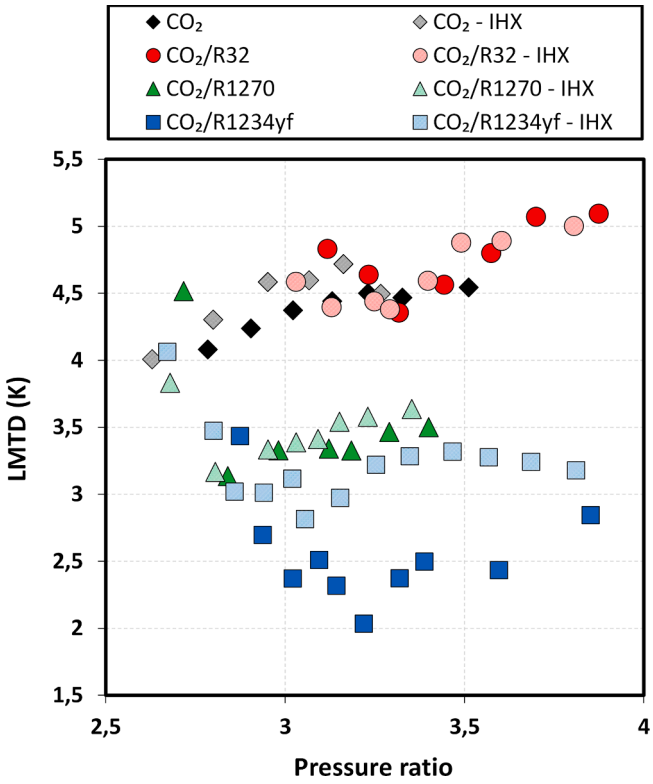

Fig. 14. $LMTD_{ev}$ vs pressure ratio.

Fig. 16 presents the evolution of the approach temperature (ΔT_{amb}) with the pressure ratio considering the presence of the IHX. As depicted, the ΔT_{amb} decreases as the pressure ratio increases, which means the

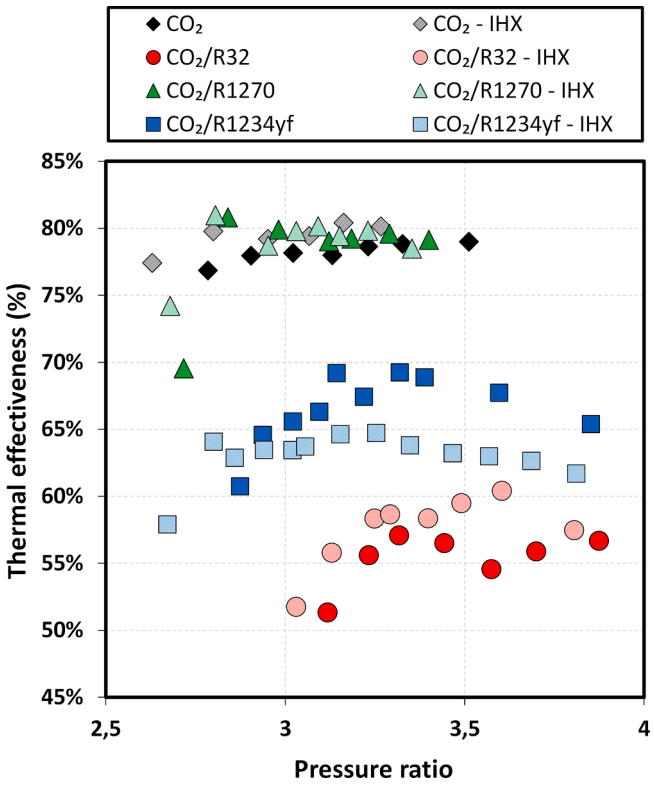

Fig. 15. ε_{ev} vs pressure ratio.

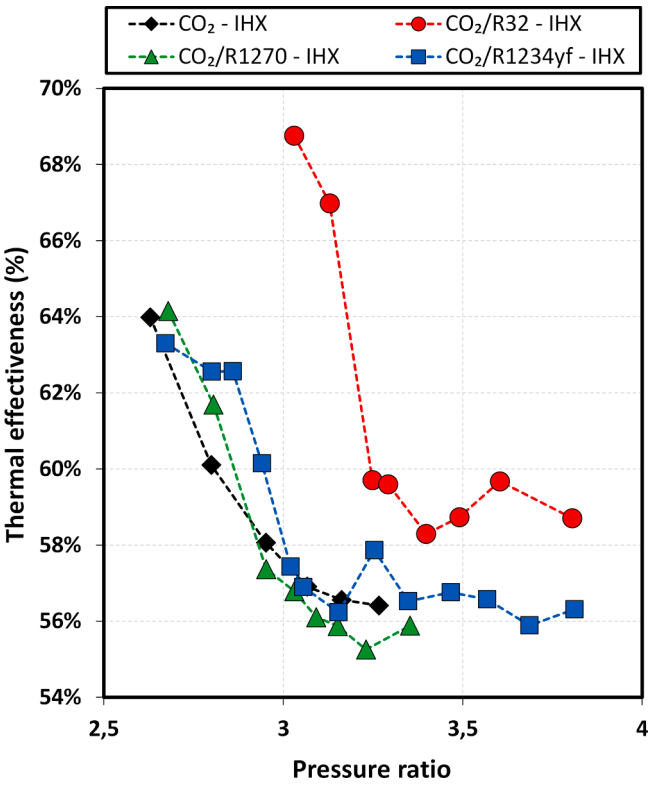

Fig. 17. ε_{ihx} vs pressure ratio.

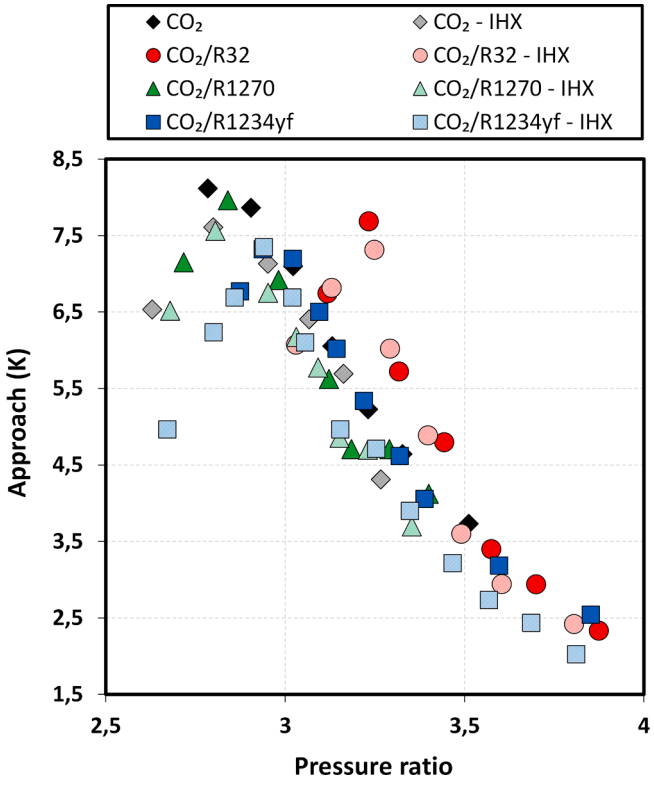

Fig. 16. Approach temperature vs pressure ratio.

condenser/gas-cooler improves its thermal effectiveness as the pressure heat rejection rises, moving from subcritical to transcritical operation. Comparing the different tested refrigerants and configurations, no noticeable differences are revealed, except for a slight approach

Table 11
Heat exchanger and compressor operation at the optimal operating conditions.

Refrigerant		ΔT_{amb} (K)	$LMTD_{ev}$ (K)	ε_{ihx} (%)	η_G (%)	η_V (%)
CO_2	without IHX	7.1	4.4	–	48.3	67.1
	with IHX	7.1	4.6	58.1	50.8	70.4
CO_2 / R32	without IHX	5.7	4.4	–	47.4	68.3
	with IHX	6.0	4.4	59.6	50.6	73.4
CO_2 / R1234yf	without IHX	4.6	2.4	–	46.4	64.9
	with IHX	5.0	3.0	56.2	48.3	67.3
CO_2 / R1270	without IHX	6.9	3.3	–	48.8	68.8
	with IHX	6.2	3.4	56.8	50.6	70.7

improvement with the IHX presence.

Concerning the thermal effectiveness of the IHX (ε_{ihx}), Fig. 17 compares the four refrigerants with an evident enhancement of the ε_{ihx} as the cycle moves from transcritical to subcritical operation. However, this is not the standard operation of the cycle since the heat rejection pressure is controlled to reach the maximum COP in the refrigerating plant, according to Table 10 or Fig. 13. Therefore, Table 11 summarizes the IHX thermal effectiveness and the other parameters discussed above at the optimal operating conditions, including the compressor parameters discussed in Section 4.6. Following Table 11, CO_2/R32 presents the highest IHX thermal effectiveness (*59.6%*) and CO_2/R1234yf the lowest (*56.2%*), but no significant difference is stated between both.

4.6. *Compressor performance*

The compressor performance is measured by the global and volumetric efficiencies (η_G and η_V) defined by the expressions Eq. (28) and Eq. (29), respectively.

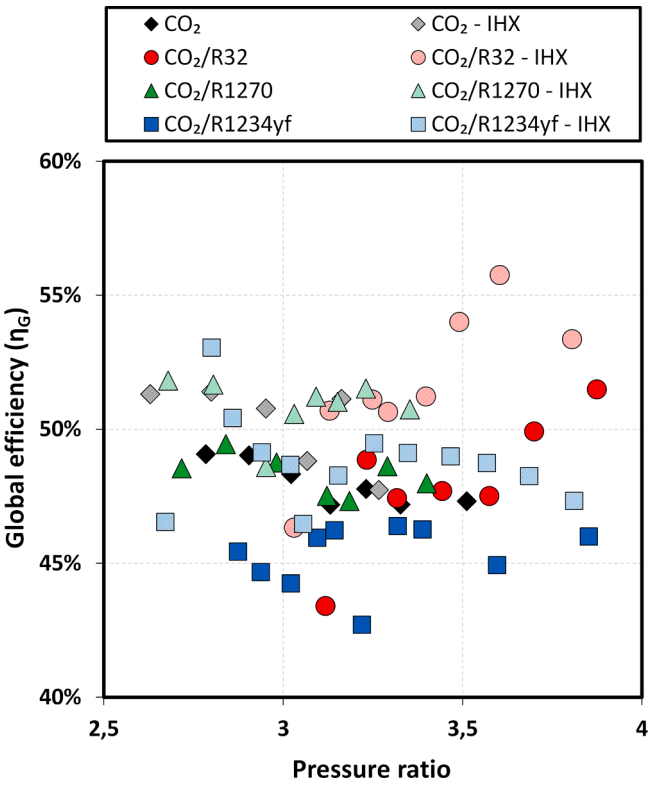

Fig. 18. Global efficiency vs pressure ratio.

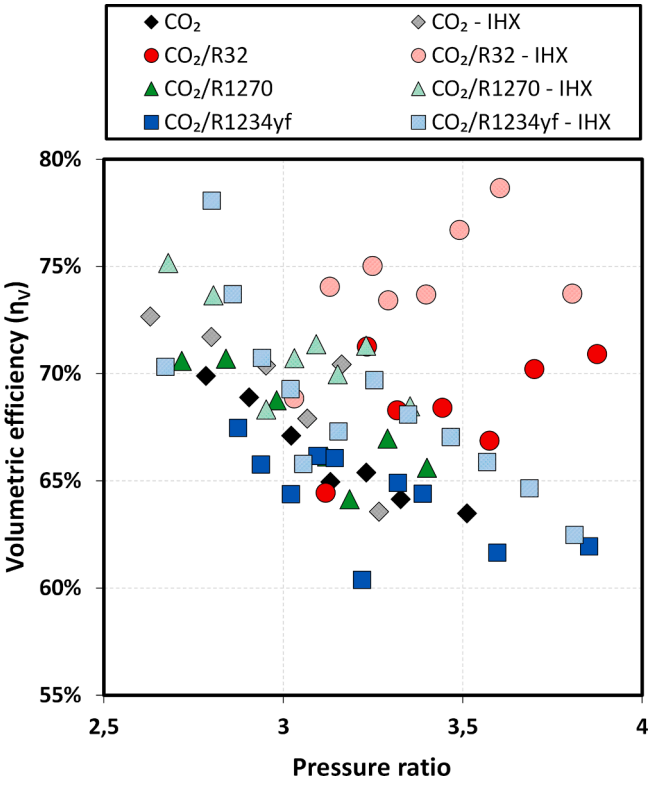

Fig. 19. Volumetric efficiency vs pressure ratio.

$$\eta_V = \frac{\dot{m}\cdot v_{suc}}{V_G\cdot N} \tag{28}$$

$$\eta_G = \frac{\dot{m}\cdot(h_{dis\ iso} - h_{suc})}{\dot{W}_c} \qquad h_{dis\ iso} = f(s_{suc}; P_{dis}) \tag{29}$$

v_{suc}, h_{suc} and s_{suc} are the specific volume, enthalpy and entropy, respectively, evaluated at the suction conditions. $h_{dis\ iso}$ is the specific enthalpy evaluated with the specific entropy at the discharge port.

Figs. 18 and 19 present the evolution of global and volumetric efficiencies with the pressure ratio, showing a slight reduction of both (higher for the volumetric one) as the higher the pressure ratio becomes. This trend differs for CO_2/R32, where the efficiencies increase unusually with the pressure ratio similar to a quadratic curve. Therefore, this behaviour could mean that both efficiencies are reaching an optimum with the pressure ratio described by Granryd *et al.* [39].

Comparing global efficiency values without IHX (Fig. 18), CO_2/R1234yf has a slightly lower global efficiency than CO_2, while CO_2/R1270 performs similarly, and CO_2/R32 works better. If the IHX is introduced, those differences become softer, and the global efficiency of CO_2 is similar to CO_2/R1234yf, while CO_2/R1270 and CO_2/R32 increase their values.

Moving to volumetric efficiency without IHX, pure CO_2 performs similarly to CO_2/R1234yf and CO_2/R1270 but lower than the mixture of CO_2/R32, as Fig. 19 shows. The use of the IHX slightly increases the volumetric efficiency values, but no significant differences were found in the trends of values.

5. Conclusions

This work determines and tests three CO_2-based mixtures with the refrigerants R32, R1270 and R1234yf, using the refrigerant CO_2 as a reference, in a transcritical refrigeration plant considering the presence of an internal heat exchanger (IHX).

The first part of the work focuses on determining the most suitable mass fraction for each mixture, considering the restrictions of GWP_{100} below 150, non-flammability conditions and maximum COP improvement. Accordingly, a computational model was developed and validated with the experimental results from CO_2, defining the best mixtures of CO_2/R32 (80.7/19.3%$_w$), CO_2/R1270 (92.4/7.6%$_w$) and CO_2/R1234yf (88/12%$_w$).

In the second part, the manuscript defines the test methodology and discusses the experimental results obtained during the test campaign. Accordingly, the defined mixtures mentioned above were tested as *drop-ins* in a small-capacity transcritical refrigeration plant equipped with a hermetic compressor and the possibility of introducing an IHX. Maintaining the same secondary fluid inlet conditions at the evaporator (0 °C and 100 kg·h^{-1}) and the condenser/gas-cooler (25 °C) and varying the heat rejection pressure, the results demonstrated the presence of a heat rejection pressure that maximises the COP of the plant. At these optimum conditions, the following results were obtained:

a) Coefficient of Performance (COP) and optimal heat rejection pressure (P_{opt})

The test results demonstrated, at the optimum conditions, COP improvements without IHX by *6.4%* with CO_2/R1270, *9.7%* with CO_2/R1234yf and *15.3%* with CO_2/R32, compared to CO_2. Moreover, the optimal heat rejection pressure values presented a reduction from *2.5* to *15.7 bar*, benefiting the refrigeration plant regulation and components design.

Testing the IHX at the same operating conditions stated above proved the benefit of introducing the IHX, with increments in COP of *6.7%* for CO_2, *12.1%* for CO_2/R1270, *16.1%* for CO_2/R1234yf and *22.2%* for CO_2/R32, taking as reference the results of CO_2 without IHX. The impact of the IHX on the optimal heat rejection pressure introduced

pressure reductions from *2.5* to *16.2 bar*, with no remarkable differences from the results obtained without IHX.

b) Cooling capacity

Working at the P_{opt} and without IHX, the effect of mixtures on the cooling capacity showed an increment by *5.1%* with CO_2/R1234yf, whit decrements by *1.9%* and *4.3%*, using CO_2/R1270 and CO_2/R32, respectively.

If the IHX is introduced, the abovementioned differences decrease, resulting in an increment of *1.3%* with CO_2/R1234yf and a reduction of *0.2%* and *1.8%* with CO_2/R1270 and CO_2/R32, respectively.

c) Compressor behaviour

Using mixtures, the compressor decreases its energy consumption due to reducing the refrigerant mass flow. The energy savings ranged from *4.2* to *17.0%* if the IHX is not used and from *4.6* to *14.2%* if the IHX is installed. Moreover, mixtures introduced slight variations in the compressor efficiencies (volumetric and global), remarking the increment caused by the CO_2/R32 on both parameters.

d) Heat exchangers operation

The impact of mixtures in the heat exchangers' performance minimised the evaporator thermal effectiveness when CO_2/R1234yf (65% on average) and CO_2/R32 (56% on average) were used, compared to CO_2 and CO_2/R1270 (80% on average). Concerning the condenser/gas-cooler, no noticeable differences were revealed, and similar temperature approaches were obtained, except for a slight improvement with the IHX presence. Finally, the effect on the IHX thermal effectiveness showed that only the CO_2/R32 mixture improved remarkably this parameter compared to CO_2 and the other fluids.

Given the results, CO_2/R32 is the most suitable mixture for a drop-in in transcritical refrigerating plants due to the COP improvement, followed by CO_2/R1234yf and CO_2/R1270. This order matches the subcritical operation of the plant when the CO_2/R32 is used as a fluid. However, it should be highlighted that using CO_2/R32 reduces the plant's cooling capacity, so a higher compressor capacity will be necessary.

Even with the good results, the present work is open for further research varying the mass fraction of the defined mixtures and the working conditions of the refrigerating plant. These tests will be covered and discussed in future incoming works.

Declaration of Competing Interest

The authors declare that they have no known competing financial interests or personal relationships that could have appeared to influence the work reported in this paper.

Data availability

Data will be made available on request.

Acknowledgements

This article is part of the project PID2021-126926OB-C21 (acronym: HELTHA), funded by the Spanish Ministry of Science and Innovation. The authors would like to acknowledge the economic support by the Ministry of Science, Innovation and Universities for the research grant PRE2019-091617 to F. Vidan-Falomir and the European Union – "NextGenerationEU" through the grant INVEST/2022/294 to R. Larrondo-Sancho.

References

[1] European Commission. Regulation (EU) No 517/2014 of the European Parliament and of the Council of 16 April 2014 on fluorinated greenhouse gases and repealing Regulation (EC) No 842/2006; 2014. https://eur-lex.europa.eu/legal-content/EN/TXT/PDF/?uri=CELEX:32014R0517.

[2] Atmosphere. Natural Refrigerants: State of the Industry. Commercial and industrial refrigeration in Europe, North America and Japan; 2022. https://atmosphere.cool/marketreport-2022/.

[3] A.F.A. Elbarghthi, V. Dvorak, A. Hafner, K. Banasiak, The potential impact of the small-scale ejector on the R744 transcritical refrigeration system, Energ Conver Manage 249 (1) (2021), 114860, https://doi.org/10.1016/j.enconman.2021.114860.

[4] L. Nebot-Andrés, D. Calleja-Anta, D. Sánchez, R. Cabello, R. Llopis, Experimental assessment of dedicated and integrated mechanical subcooling systems vs parallel compression in transcritical CO_2 refrigeration plants, Energ Conver Manage 252 (15) (2022), 115051, https://doi.org/10.1016/j.enconman.2021.115051.

[5] P. Gullo, B. Elmegaard, G. Cortella, Energy and environmental performance assessment of R744 booster supermarket refrigeration systems operating in warm climates, Int J Refrig 64 (2016) 61–79, https://doi.org/10.1016/j.ijrefrig.2015.12.016.

[6] F. Fazelpour, T. Morosuk, Exergoeconomic analysis of carbon dioxide transcritical refrigeration machines, Int J Refrig 38 (2014) 128–139, https://doi.org/10.1016/j.ijrefrig.2013.09.016.

[7] D. Sánchez, A. Andreu-Nácher, D. Calleja-Anta, R. Llopis, R. Cabello, Energy impact evaluation of different low-GWP alternatives to replace R134a in a beverage cooler. Experimental analysis and optimization for the pure refrigerants R152a, R1234yf, R290, R1270, R600a and R744, Energ Conver Manage 256 (15) (2022), 115388, https://doi.org/10.1016/j.enconman.2022.115388.

[8] S.G. Kim, M.S. Kim, Experiment and simulation of the performance of an autocascade refrigeration system using carbon dioxide as a refrigerant, Int J Refrig 25 (2001) 1093–1101, https://doi.org/10.1016/S0140-7007(01)00110-4.

[9] G. Di Nicola, G. Giuliani, F. Polonara, R. Stryjek, Blends of carbon dioxide and HFCs as working fluids for the low-temperature circuit in cascade refrigerating systems, Int J Refrig 28 (2005) 130–140, https://doi.org/10.1016/j.ijrefrig.2004.06.014.

[10] B. Niu, Y. Zhang, Experimental study of the refrigeration cycle performance for the R744/R290 mixtures, Int J Refrig 30 (1) (2007) 37–42, https://doi.org/10.1016/j.ijrefrig.2006.06.002.

[11] J.H. Kim, J.M. Cho, M.S. Kim, Cooling performance of several CO_2/propane mixtures and glide matching with secondary heat transfer fluid, Int J Refrig 31 (5) (2008) 800–806, https://doi.org/10.1016/j.ijrefrig.2007.11.009.

[12] B. Dai, C. Dang, M. Li, H. Tian, Y. Ma, Thermodynamic performance assessment of carbon dioxide blends with low-global warming potential (GWP) working fluids for a heat pump water heater, Int J Refrig 56 (2015) 1–14, https://doi.org/10.1016/j.ijrefrig.2014.11.009.

[13] P. Bouteiller, P. Tobaly, M.F. Terrier, A Methodology and bench design for experimental study of heat pump thermodynamic cycles using CO_2 based mixtures, in: 12th IIR Gustav Lorentzen Conference on Natural Refrigerants (GL2016). Proceedings. Édimbourg, United Kingdom, August 21st-24th 2016, 2016, https://doi.org/10.18462/iir.gl.2016.1015.

[14] P. Bouteiller, M.F. Terrier, P. Tobaly, Experimental study of heat pump thermodynamic cycles using CO_2 based mixtures - methodology and first results, AIP Conf Proc 1814 (2017), 020052, https://doi.org/10.1063/1.4976271.

[15] D. Wang, Y. Lu, L. Tao, Thermodynamic analysis of CO_2 blends with R41 as an azeotropy refrigerant applied in small refrigerated cabinet and heat pump water heater, Appl Therm Eng 125 (2017) 1490–1500, https://doi.org/10.1016/j.applthermaleng.2017.07.009.

[16] P. Tobaly, M.F. Terrier, P. Bouteiller, CO^{2+} propane mixture as working fluid for refrigeration in hot climates. Experimental results of energy efficiency tests, in: 13th IIR Gustav Lorentzen conference on natural refrigerants: natural refrigerant solutions for warm climate, 2018, pp. 18–20, https://doi.org/10.18462/iir.gl.2018.1276.

[17] B. Yu, D. Wang, C. Liu, F. Jiang, J. Shi, J. Chen, Performance improvements evaluation of an automobile air conditioning system using CO_2-propane mixture as a refrigerant, Int J Refrig 88 (2018) 172–181, https://doi.org/10.1016/j.ijrefrig.2017.12.016.

[18] B. Yu, J. Yang, D. Wang, J. Shi, Z. Guo, J. Chen, Experimental energetic analysis of CO_2/R41 blends in automobile air conditioning and heat pump systems, Appl Energy 239 (2019) 1142–1153, https://doi.org/10.1016/j.apenergy.2019.02.028.

[19] L.H.P. Massuchetto, R.B.C. do Nascimento, S.M.R. de Carvalho, H.V. de Araújo, J. V.H. d'Angelo, Thermodynamic performance evaluation of a cascade refrigeration system with mixed refrigerants: R744/R1270, R744/R717 and R744/RE170, Int J Refrig 106 (2019) 201–212, https://doi.org/10.1016/j.ijrefrig.2019.07.005.

[20] Z. Sun, Q. Cui, Q. Wang, J. Ning, J. Guo, B. Dai, Y. Liu, Y. Xu, Experimental study on CO_2/R32 blends in a water-to-water heat pump system, Appl Therm Eng 162 (2019), 114303, https://doi.org/10.1016/j.applthermaleng.2019.114303.

[21] D. Sánchez, F. Vidan-Falomir, L. Nebot-Andrés, R. Llopis, R. Cabello, Alternative blends of CO_2 for transcritical refrigeration systems. Experimental approach and energy analysis, Energ Conver Manage 279 (1) (2023), 116690, https://doi.org/10.1016/j.enconman.2023.116690.

[22] G. Vaccaro, A. Milazzo, L. Talluri, Thermodynamic assessment of trans-critical refrigeration systems utilizing CO_2-based mixtures, Int J Refrig 147 (2023) 61–70, https://doi.org/10.1016/j.ijrefrig.2022.09.013.

[23] M. Martínez-Angeles, E. Sicco, G. Toffoletti, L. Nebot-Andrés, D. Sánchez, R. Cabello, G. Cortella, R. Llopis, Evaluation of CO_2-doped blends in single-stage

with IHX and parallel compression refrigeration architectures. Int J Refrig. In Press Journal Pre-proof (2023) https://doi.org/10.1016/j.ijrefrig.2023.03.009.
[24] D. Sánchez, F. Vidan-Falomir, R. Larrondo-Sancho, R. Llopis, R. Cabello, Alternative CO_2-based blends for transcritical refrigeration systems, Int J Refrig. In press Journal Pre-proof (2023), https://doi.org/10.1016/j.ijrefrig.2023.03.021.
[25] E. Torrella, D. Sánchez, R. Llopis, R. Cabello, Energetic evaluation of an internal heat exchanger in a CO_2 transcritical refrigeration plant using experimental data, Int J Refrig 34 (1) (2011) 40–49, https://doi.org/10.1016/j.ijrefrig.2010.07.006.
[26] J. M. Calm, ARTI refrigerant database. Data summaries - Volume 1: single-compound refrigerants. Air Conditioning and Refrigeration Technology Institute; 1999. Reference: DOE/CE/23810-105.
[27] Honeywell. HFO-1234yf Low GWP Refrigerant Update. International Refrigeration and Air Conditioning Conference; 2008. https://www.honeywellrefrigerants.com/india/?document=2008-purdue-conference-low-gwp-refrigerants&download=1.
[28] IPCC. Climate Change 2022: Impacts, Adaptation, and Vulnerability. Contribution of Working Group II to the Sixth Assessment Report of the Intergovernmental Panel on Climate Change. In: Pörtner H-O, Roberts DC, Tignor M, Poloczanska ES, Mintenbeck K, Alegría A, Craig M, Langsdorf S, Löschke S, Möller V, Okem A, Rama B, editors. Cambridge, UK and New York, NY, USA: Cambridge University Press; 2022. 3056 pp., 10.1017/9781009325844.
[29] Ø. Hodnebrog, S.B. Dalsøren, G. Myhre, Lifetimes, direct and indirect radiative forcing, and global warming potentials of ethane (C_2H_6), propane (C_3H_8), and butane (C_4H_{10}), Atmos Sci Lett 19 (2) (2018) e804.
[30] ASHRAE, Standard 34-2019. Designation and safety classification of refrigerants; 2019.
[31] R.S. Agarwal, E. Clark, Refrigerant blends: calculating Global Warming Potentials, UNEP. Reference OZFS/16/04-10 rev2. https://wedocs.unep.org/bitstream/handle/20.500.11822/28320/7786RefBlends_EN.pdf?sequence=1&isAllowed=y.
[32] S. Kondo, K. Takizawa, A. Takahashi, K. Tokuhashi, Extended Le Chatelier's formula for carbon dioxide dilution effect on flammability limits, J Hazard Mater A138 (2006) 1–8, https://doi.org/10.1016/j.jhazmat.2006.05.035.
[33] I.H. Bell, E.W. Lemmon, Automatic fitting of binary interaction parameters for multi-fluid HelmholtzEnergy-explicit mixture models, J Chem Eng Data 61 (2016) 3752–3760. https://pubs.acs.org/doi/pdf/10.1021/acs.jced.6b00257.
[34] G. Raabe, Molecular simulation studies on the vapor−liquid phase equilibria of binary mixtures of R-1234yf and R-1234ze(E) with R-32 and CO_2, J Chem Eng Data 58 (2013) 1867–1873. https://pubs.acs.org/doi/pdf/10.1021/je4002619?src=getftr.
[35] D. Sánchez, J. Catalán-Gil, R. Cabello, D. Calleja-Anta, R. Llopis, L. Nebot-Andrés, Experimental analysis and optimization of an R744 transcritical cycle working with a mechanical subcooling system, Energies 13 (12) (2020) 3204, https://doi.org/10.3390/en13123204.
[36] W.J. Mulroy, P.A. Domanski, D.A. Didion, Glide matching with binary and ternary zeotropic refrigerant mixtures Part 1. An experimental study, Int J Refrig 17 (4) (1994) 220–225, https://doi.org/10.1016/0140-7007(94)90037-X.
[37] R. Cabello, D. Sánchez, E. Torrella, R. Llopis, Experimental evaluation of the energy efficiency of a CO_2 refrigerating plant working in transcritical conditions, Appl Therm Eng 28 (13) (2008) 1596–1604, https://doi.org/10.1016/j.applthermaleng.2007.10.026.
[38] Y. Zhu, X. Wu, Z. Wei, Heat transfer characteristics and correlation for CO_2/propane mixtures flow evaporation in a smooth mini tube, Appl Therm Eng 81 (2015) 253–261, https://doi.org/10.1016/j.applthermaleng.2015.02.009.
[39] E. Granryd, I. Ekroth, P. Lundqvist, Å. Melinder, B. Palm, P. Rohlin, Refrigeration Engineering, of Energy Technology. Division of Applied Thermodynamics and Refrigeration, 5th ed., Department, Stockholm (Sweden, 978-91-7415-415-3), 2009.